

THE INTERNAL-COLLISION-INDUCED MAGNETIC RECONNECTION AND TURBULENCE (ICMART) MODEL OF GAMMA-RAY BURSTS

BING ZHANG¹, HUIRONG YAN^{2,3}

Draft version October 31, 2018

ABSTRACT

The recent Fermi observation of GRB 080916C shows that the bright photosphere emission associated with a putative fireball is missing, which suggests that the central engine likely launches a Poynting-flux-dominated outflow. We propose a model of gamma-ray burst (GRB) prompt emission in the Poynting-flux-dominated regime, namely, the Internal-Collision-induced MAgnetic Reconnection and Turbulence (ICMART) model. It is envisaged that the GRB central engine launches an intermittent, magnetically-dominated wind, and that in the GRB emission region, the ejecta is still moderately magnetized (e.g. $1 \lesssim \sigma \lesssim 100$). Similar to the internal shock (IS) model, the mini-shells interact internally at the radius $R_{\text{IS}} \sim \Gamma^2 c \Delta t$. Most of these early collisions, however, have little energy dissipation, but serve to distort the ordered magnetic field lines entrained in the ejecta. At a certain point, the distortion of magnetic field configuration reaches the critical condition to allow fast reconnection seeds to occur, which induce relativistic MHD turbulence in the interaction regions. The turbulence further distorts field lines easing additional magnetic reconnections, resulting in a runaway release of the stored magnetic field energy (an ICMART event). Particles are accelerated either directly in the reconnection zone, or stochastically in the turbulent regions, which radiate synchrotron photons that power the observed gamma-rays. Each ICMART event corresponds to a broad pulse in the GRB light curve, and a GRB is composed of multiple ICMART events. This model retains the merits of the IS and other models, but may overcome several difficulties/issues faced by the IS model (e.g. low efficiency, fast cooling, electron number excess, Amati/Yonetoku relation inconsistency, and missing bright photosphere). Within this model, the observed GRB variability time scales could have two components, one slow component associated with the central engine time history, and another fast component associated with relativistic magnetic turbulence in the emission region. The model predicts a decrease of gamma-ray polarization degree and E_p in each ICMART event (broad pulse) during the prompt GRB phase, as well as a moderately magnetized external reverse shock. The model may be applied to the GRBs that have time-resolved, featureless Band-function spectra, such as GRB 080916C and most GRBs detected by Fermi LAT.

Subject headings: gamma-rays burst: general – gamma-ray bursts: individual: GRB 080916C – magnetic reconnection – turbulence

1. INTRODUCTION

The composition of the Gamma-Ray Burst (GRB) ejecta has remained a mystery until recently. The uncertainty lies in the lack of knowledge about the ratio between Poynting flux and matter (baryonic) flux⁴, i.e.⁵

$$\sigma = \frac{F_P}{F_b} = \frac{B^2}{4\pi\Gamma\rho c^2} = \frac{B'^2}{4\pi\rho'c^2}, \quad (1)$$

where B and ρ are the magnetic field strength and matter density in the rest frame of the central engine

(or the lab frame), and B' and ρ' are the corresponding quantities in the rest frame comoving with the ejecta. The standard picture is the “fireball” shock model (Paczýnski 1986; Goodman 1986; Shemi and Piran 1990; Rees and Mészáros 1992; Mészáros and Rees 1993; Rees and Mészáros 1994). Within such a picture, an initially hot fireball composed of photons, electron-positron pairs, and a small amount of baryons first converts most of its thermal energy into kinetic energy, and then dissipates the kinetic energy in the internal (or sometimes external) shocks to power the observed GRB emission. Within such a scenario, the magnetic field is assumed not to play a dynamically important role in the ejecta, i.e. $\sigma \ll 1$. Such a field can be generated *in-situ* via plasma instabilities (Weibel 1959; Medvedev and Loeb 1999; Nishikawa et al. 2005, 2009; Spitkovsky 2008) in relativistic shocks, in which Fermi-accelerated electrons cool via synchrotron/jitter (Mészáros et al. 1994; Tavani 1996; Medvedev 2000) or synchrotron self-Compton (SSC) (Mészáros et al. 1994; Kumar and McMahon 2008) radiation. An alternative view is that the GRB ejecta carries a dynamically important magnetic field component, i.e. $\sigma \gg 1$. The GRB radiation is powered by dissipation of the magnetic field energy in the ejecta (Usov 1992; Thompson 1994; Mészáros and Rees 1997b;

¹ Department of Physics and Astronomy, University of Nevada Las Vegas, Las Vegas, NV 89154.

² Kavli Institute of Astronomy and Astrophysics, Peking University, Beijing 100871, China.

³ TAP Fellow, University of Arizona, 1629 E. University Blvd., Tucson, AZ, 85721.

⁴ Strictly speaking, the matter flux is the sum of the baryonic flux and the leptonic flux. It is usually dominated by the baryonic flux unless the pair number density is so high that $N_{\pm}/N_b \geq m_p/m_e$ is satisfied.

⁵ The last equation applies to the case that the magnetic field lines are perpendicular to the direction of the motion, which is the configuration invoked in the ICMART model proposed in this paper. If magnetic fields are generated in the internal shocks due to plasma instabilities, the comoving field lines would have random orientations. In this case, one has $\sigma \simeq B'^2/8\pi\rho'c^2$.

Lyutikov and Blandford 2003; Vlahakis and Königl 2003; Lazarian et al. 2003; Lyutikov 2006a).

Until recently, it has been difficult to diagnose the composition of GRB ejecta. Regardless of the σ values, the late time afterglow behavior appears the same, which is the emission of the “forwardly” shocked circumburst medium. Successful modeling of some afterglow data therefore does *not* shed light onto the composition of the ejecta. An important phase is when the ejecta energy is transferred to the circumburst medium. This is usually accompanied by passing of a reverse shock across the ejecta (Sari and Piran 1995; Zhang and Kobayashi 2005). The brightness of the reverse shock emission is found to be dependent on the magnetization parameter (Fan et al. 2004a; Zhang and Kobayashi 2005; Mizuno et al. 2009a; Mimica et al. 2009). However, both low- σ and high- σ flows can lead to a relatively dim reverse shock emission (Zhang and Kobayashi 2005; Jin and Fan 2007), so that it is difficult to robustly constrain σ from the observations of the reverse shock emission. Finally, the prompt emission light curves and the narrow-band spectra (in the energy bands of the previous gamma-ray detectors such as BATSE, Swift, etc) may be accommodated within the frameworks of both the low- σ (internal shock) and high- σ (magnetic dissipation) models, so that they do not carry adequate information to diagnose GRB composition. The progress in constraining GRB composition therefore has been slow.

In any case, it has been long speculated that the GRB ejecta are somewhat magnetized. The putative GRB central engines, either a black hole - torus system (e.g. Proga et al 2003) or a rapidly spinning neutron star (e.g. Usov 1992), are very likely magnetized. The GRB ejecta is likely entrained with a globally structured magnetic field. In principle, the σ factor can reach ~ 1 or even $\gg 1$. Before the launch of Fermi, several authors have argued for a strongly magnetized GRB central engine based on some observational evidence and its theoretical modeling. Coburn and Boggs (2003) reported a $80\% \pm 20\%$ degree of linear polarization in GRB 021206, which is best interpreted by synchrotron emission in a globally structured magnetic field (Waxman 2003; Lyutikov et al. 2003; Granot 2003). However, a further analysis of the same data cannot confirm the claim (Rutledge and Fox 2004). By modeling early optical flashes within the reverse shock model, Zhang et al. (2003) found that the early optical flashes with a rapidly decaying light curve (reverse shock component) followed by a flattening feature (forward shock) as observed in GRB 990123 and GRB 021211 generally require that the reverse shock region is much more magnetized than the forward shock region. Such a conclusion was independently drawn by Fan et al. (2002) and Kumar and Panaitescu (2003) through detailed case studies of the two GRBs. This extra magnetization has to be related to a magnetized central engine. More recently, Kumar and McMahon (2008); Kumar and Panaitescu (2008) analyzed the prompt emission data of several GRBs based on a largely model-independent method. They concluded that the observed emission cannot be produced by synchrotron emission within the internal shock model. They tentatively suggested a magnetized ejecta as the source of the observed gamma-ray radiation.

Recent Fermi observations shed light onto the composition of some GRBs. Fermi carries the Gamma-ray Burst Monitor (GBM) and the Large Area Telescope (LAT), which cover a broad spectral range of 6-7 orders of magnitude in energy. It is ideal to measure the broad-band spectra of GRBs during the prompt emission phase. The first bright GRB co-detected by GBM and LAT, GRB 080916C, showed several nearly featureless, smoothly-joint-broken-power-law spectra (the so-called “Band”-function, Band et al. (1993)) covering 6-7 decades in energy (Abdo et al. 2009; Zhang et al. 2010). Although this might not be surprising for observers (the Band-function has been known since the early BATSE years), it was somewhat surprising for modelers, since according to the standard fireball model, a thermal component associated with the fireball “photosphere” is expected to be very bright and should be detected (Zhang and Pe’er 2009). This component is analogous to the cosmic microwave background radiation (CMB) associated with the hot Big Bang, and is predicted to be bright enough to be detectable within a wide range of parameters (Mészáros and Rees 2000; Mészáros et al. 2002; Pe’er et al. 2006; Pe’er 2008). Zhang and Pe’er (2009) analyzed this burst and argued that the non-detection of the thermal component strongly suggests that the majority of energy (more than 95%) was not stored in the form of a “fireball” at the central engine, but was stored in magnetic fields which was not released until reaching a large radius. This suggests that at least for GRB 080916C the outflow has to be *Poynting flux dominated* (PFD) with $\sigma > (15 - 20)$ at the central engine and at the photosphere as well. A follow up investigation (Fan 2010) on the various possibilities of hiding the thermal component (e.g. by invoking a smaller central engine radius, which is not required by the minimum variability time scale data of GRB 080916C) confirms the conclusion (see also Gao et al. 2009)⁶. All these call for a serious re-investigation of GRB prompt emission models in the high- σ regime.

In this case, magnetic energy may be sufficient to feed GRBs. Magnetic reconnection was suggested as a component for GRBs long ago (Thompson 1994). The problem lied, however, in the intrinsic difficulty of reconnection as it is a very slow process in ordered fields. As with the case for solar flares, both a slow phase of accumulation of the oppositely directed flux and a fast bursty phase are required for reconnection. Essential progress was made by (Lazarian et al. 2003), who proposed a new scenario for GRBs by invoking self-adjusted reconnection based on the findings of fast reconnection in 3D turbulent magnetic fields (Lazarian and Vishniac 1999). They suggested that the fast bursty reconnection eventually occurs as a nonlinear feedback of the increased stochasticity of the magnetic field lines. The reconnection events start from some limited volumes and then spread in the form of a chain reaction as the energy is fed back to the turbulence and induces dramatic change in the magnetic field topology. The turbulent reconnection model has

⁶ An alternative model is to interpret the entire spectra as the emission from a dissipative fireball photosphere (Beloborodov 2010; Lazzati and Begelman 2010). This model, although plausible to interpret some GRBs, is found to be difficult to interpret the data of GRB 080916C, see (Zhang et al. 2010) and Sect.2.3 for a more detailed discussion).

been confirmed by recent numerical testings (Kowal et al. 2009).

In this paper, we build a model of GRB prompt emission in the high- σ regime on the basis of the recent observational and theoretical achievements. This model is called the *Internal-Collision-induced MAgnetic Recon-nection and Turbulence* (ICMART) model. In §2, we critically review the current prompt emission models, including the internal shock (IS) model (§2.1) in the low- σ regime, the electro-magnetic model in the extremely high- σ regime (§2.2) and the dissipative photosphere model in the low- to intermediate- σ regime (§2.3). We argue that these models are not ideal to interpret GRB 080916C and some other GRBs. We then delineate the general picture of the ICMART model in §3. In §4 we discuss the merits of the ICMART model, focusing on how it inherits the merits of the previous models and overcomes their drawbacks. In §5, we outline several unique predictions of the ICMART model, which can be used to differentiate this model from other models based on the observational data. These include the existence of two variability components, an evolution of E_p and gamma-ray polarization degree across each GRB pulse, as well as a mildly polarized external reverse shock emission from GRBs. We then dedicate §6 discussing how the ICMART model interprets the observation of GRB 080916C. The ICMART model is summarized in §7 with some discussion on its broad implications on other aspects of GRB physics (e.g. neutrino and cosmic ray connections with GRBs) as well as its possible applications to other astrophysical objects such as active galactic nuclei (AGNs). The physics invoked in this model (e.g. turbulence and reconnection in a high- σ , relativistic plasma) is complicated. In this paper we make the first step by delineating the qualitative picture of the model, and defer the more detailed quantitative/numerical analyses to future work.

2. PREVIOUS GRB PROMPT EMISSION MODELS

2.1. The internal shock model

For a baryonic outflow ($\sigma \ll 1$), the standard GRB prompt emission model is the internal shock (IS) model (Rees and Mészáros 1994; Paczyński and Xu 1994). It is envisioned that the GRB central engine launches an unsteady outflow with varying luminosity and Lorentz factors. Approximating the outflow as a series of “mini-shells” with a distribution of Lorentz factors [$\Gamma \in (\Gamma_{\min}, \Gamma_{\max})$], widths [$\Delta \in (\Delta_{\min}, \Delta_{\max}) = (c\Delta t_{\min}, c\Delta t_{\max})$, where Δt is the duration of the central engine activity of each minishell], and separations [$d \in (d_{\min}, d_{\max}) = (c\delta t_{\min}, c\delta t_{\max})$, where δt is the duration between the end of ejecting a leading shell and the beginning of ejecting a trailing shell], one can obtain a series of collisions due to the interactions between the late, fast shells and the early, slow shells. These collisions are supersonic, resulting in internal shocks from which particles are accelerated and photons are released to power the GRB prompt emission. For two shells with parameters (Γ_s, Δ_s) and (Γ_f, Δ_f) separated by $d = c\delta t$ (with the fast shell lagging behind the slow shell), the internal shock radius is (noticing $\beta = (1 - \Gamma^{-2})^{1/2}$)

$$R_{\text{IS}} = \frac{d}{\beta_f - \beta_s} \simeq 2\Gamma_s^2 c\delta t = 6 \times 10^{14} \text{ cm } \Gamma_{s,2.5}^2 \delta t_{-1}, \quad (2)$$

where $\Gamma_{s,2.5} = \Gamma_s/10^{2.5}$. Hereafter the convention $Q_s = Q/10^s$ is adopted in cgs units throughout the text.

2.1.1. Merits: central-engine-driven variability

Most GRB light curves are highly variable. The internal shock model attributes this variability to that of the central engine. Internal collisions are also frequently observed or inferred from other astronomical objects, such as pulsar wind nebula, AGN, and planetary nebulae. It is therefore natural to envision internal collisions in GRBs as well. The connection between the observed GRB variability and that of the GRB central engine is recently strengthened by the observations and modeling of X-ray flares found in some Swift GRBs (Burrows et al. 2005; Falcone et al. 2006; Romano et al. 2006; Chincarini et al. 2007; Falcone et al. 2007), which are believed to be due to late central engine activities (Burrows et al. 2005; Zhang et al. 2006; Fan and Wei 2005; Lazzati and Perna 2007; Maxham and Zhang 2009). A strong support to such an interpretation was presented by Liang et al. (2006), who blindly searched for T_0 of the flares based on the high-latitude “curvature” effect model of the decaying phase of the flares using the observed temporal and spectral data. They found that the required T_0 are often near the beginning of the flares, which strongly suggests that the GRB central engine is restarted. Since X-ray flares and gamma-ray pulses share the same origin, as is demonstrated by the smooth transition between the two phases (e.g. Krimm et al. 2007), the GRB/X-ray flare data in general demand that the observed variability in GRBs should be tied to that of the central engine. The internal shock model naturally makes such a connection, i.e. the observed variability time history roughly traces the time history of the central engine (Kobayashi et al. 1997; Maxham and Zhang 2009). Furthermore, it has been argued that the radiation efficiency of the internal shock model can be much higher than that of the external shock model to interpret variable light curves (Sari and Piran 1997) cf. (Dermer and Mitman 1999) (but still not efficient enough to interpret the data, see below). This has made the IS model a popular theoretical model for GRB prompt emission for many years.

Despite of its popularity, the IS model suffers from several criticisms, which we summarize in the following.

2.1.2. The efficiency problem

Suppose that the second, fast shell (m_2, Γ_2) catches up with the first, slow shell (m_1, Γ_1), and that the two shells undergo a full inelastic collision and generate an internal energy U' . From energy conservation, $\Gamma_1 m_1 + \Gamma_2 m_2 = \Gamma_m (m_1 + m_2 + U'/c^2)$, and momentum conservation, $\Gamma_1 \beta_1 m_1 + \Gamma_2 \beta_2 m_2 = \Gamma_m \beta_m (m_1 + m_2 + U'/c^2)$, one can derive the Lorentz factor of the merged shell

$$\Gamma_m = \left(\frac{\Gamma_1 m_1 + \Gamma_2 m_2}{m_1/\Gamma_1 + m_2/\Gamma_2} \right)^{1/2}. \quad (3)$$

The energy dissipation efficiency (which is the upper limit of the radiation efficiency when the “fast cooling” condition is satisfied) of the collision is

$$\eta_{\text{hs}} = \frac{\Gamma_m U'}{\Gamma_1 m_1 c^2 + \Gamma_2 m_2 c^2}$$

$$= 1 - \frac{m_1 + m_2}{\sqrt{m_1^2 + m_2^2 + m_1 m_2 \left(\frac{\Gamma_2}{\Gamma_1} + \frac{\Gamma_1}{\Gamma_2} \right)}}. \quad (4)$$

This efficiency is typically low (Kobayashi et al. 2007; Panaitescu et al. 1999; Kumar 1999). The most efficient collisions are those with equal masses and large Γ ratios, but for a distribution of mass and Lorentz factor of a group of randomly ejected shells, the mean efficiency is low, e.g. $< 15\%$ for $\Gamma_{\max}/\Gamma_{\min} < 100$. For a standard electron equipartition parameter $\epsilon_e \sim 0.1$, this model predicts an X-ray afterglow flux brighter than the observed flux by near 3 orders of magnitude (Maxham and Zhang 2009). Increasing η_{IS} requires adjusting the Lorentz factor distribution of the shells, so that the Γ contrast is systematically increased (Beloborodov 2000; Kobayashi and Sari 2001; Guetta et al. 2001). There is no obvious physical reason why GRB central engines would satisfy these contrived requirements. Observationally, a detailed study of the GRB radiative efficiency based on the Swift BAT/XRT data of a sample of GRBs (Zhang et al. 2007) suggests that the radiative efficiency of some GRBs can be as high as 90%. This is difficult to interpret within the straightforward IS models.

2.1.3. The fast cooling problem

In the internal shock scenario, once an electron is accelerated at the shock front, it would cool rapidly downstream through synchrotron/SSC emission. A typical GRB has an observed peak energy $E_p \sim 250$ keV. This can be translated into an estimate of the typical electron Lorentz factor $\gamma_{e,p}$ that contributes to E_p . Within the standard synchrotron emission model, one has

$$E_p \sim \hbar \Gamma \gamma_{e,p}^2 \frac{eB'}{m_e c} (1+z)^{-1}, \quad (5)$$

where Γ is the bulk Lorentz factor of the shocked region (Γ_m in Eq.[3] for an individual collision in the IS model); B' is the magnetic field strength in the comoving frame. For an outflow (or “wind”) with a mean kinetic luminosity L_w , the total internal energy due to shock dissipation is $L_w \eta_{\text{IS}}$. Assuming that this internal energy is distributed to protons, electrons and magnetic fields in the fractions ϵ_p , ϵ_e and ϵ_B , with $\epsilon_p + \epsilon_e + \epsilon_B = 1$, one has $(L_w \eta_{\text{IS}} \epsilon_B)/(4\pi R^2 c \Gamma^2) = B'^2/8\pi$, so that $\Gamma B' = (2L_w \eta_{\text{IS}} \epsilon_B/cR^2)^{1/2}$. As will be evidenced soon below, the emission is in the “fast cooling” regime so that the energy distributed to electrons is essentially converted to the observed gamma-rays. The (isotropic) gamma-ray luminosity (a direct observable) can be approximated as $L_\gamma = L_w \eta_{\text{IS}} \epsilon_e$. Taking a typical redshift $z = 1$, Eq.(5) gives the constraint

$$\gamma_{e,p} \simeq 2.3 \times 10^3 L_{\gamma,52}^{-1/4} R_{14}^{1/2} \times \left(\frac{\epsilon_e}{\epsilon_B} \right)^{1/4} \left(\frac{1+z}{2} \right)^{1/2} \left(\frac{E_p}{250 \text{ keV}} \right)^{1/2}. \quad (6)$$

The comoving cooling time scale for an electron with Lorentz factor γ_e is $t'_c(\gamma_{e,p}) = (\gamma_e m_e c^2)/[(4/3)\gamma_e^2 \sigma_T c (B'^2/8\pi)(1+\mathcal{Y})] = (6\pi m_e c)/[\gamma_e \sigma_T B'^2(1+\mathcal{Y})] = 0.008 s \gamma_{e,3}^{-1} B_4'^{-2} (1+\mathcal{Y})^{-1}$, where $\mathcal{Y} = U'_{\text{ph}}/U'_B$ is the ratio between the comoving photon energy density

and the magnetic density. Comparing with the comoving dynamical time scale $t'_{\text{dyn}} = R/\Gamma c \sim 110 s R_{15} \Gamma_{2.5}^{-1}$, one has $t'_c(\gamma_{e,p}) \ll t'_{\text{dyn}}$. This suggests that electrons at $\gamma_{e,p}$ cool rapidly within the dynamical time, forming an electron spectrum of $N(\gamma_e) \propto \gamma_e^{-2}$ below $\gamma_{e,p}$ all the way to $\gamma_{e,c} \sim 1 \ll \gamma_{e,p}$ for the nominal parameters adopted. One therefore expects that the photon number density below E_p follows $N(E) \propto E^{-3/2}$ (Sari et al. 1998). This is different from the typical low energy photon spectrum observed in most GRBs, $N(E) \propto E^\alpha$, with $\alpha \sim -1$ (Preece et al. 2000). This is the “fast cooling problem” of the IS model (Ghisellini et al. 2000). A similar argument from a different approach was presented in Kumar and McMahon (2008). Since it stems from the synchrotron cooling argument in general, this problem applies to all the scenarios in which electrons are accelerated only once without continuous heating, such as the shock acceleration scenario commonly discussed in the literature. Possibilities to alleviate this problem within the IS model include introducing decay of the shock generated magnetic fields (Pe’er and Zhang 2006) and introducing 2nd order stochastic Fermi acceleration in the post shock region due to plasma turbulence (Asano and Terasawa 2009).

2.1.4. The electron number excess problem

In the internal shock model, if all the electrons associated with the ejecta are accelerated, for typical parameters one has too many electrons to share the dissipated internal energy, so that the typical synchrotron emission frequency is smaller than what is observed by ~ 2 orders of magnitude. The argument is the following.

Since the synchrotron spectrum for the internal shock scenario is in the fast cooling regime, E_p should be defined by synchrotron emission of the minimum energy electrons injected at the shock front, i.e. $\gamma_{e,p} = \gamma_{e,m}$. The mean proton Lorentz factor $\bar{\gamma}_p$ depends on the parameters (m, Γ) of the two colliding shells, and the relative Lorentz factor between the two shells $\Gamma_{fs} = (\Gamma_f/\Gamma_s + \Gamma_s/\Gamma_f)/2$. Rigorously, one can divide the shock interaction region into 4 regions (1: unshocked leading shell; 2: shocked leading shell; 3: shocked trailing shell; 4: unshocked trailing shell). The reverse shock is typically stronger than the forward shock, which is more relevant to GRB prompt emission. For a rough estimate, one has

$$\bar{\gamma}_p - 1 \simeq (\Gamma_{43} - 1)\epsilon_p, \quad (7)$$

where Γ_{43} is related to Γ_{fs} and the parameters (m, Γ) of the two colliding shells. This can be reduced to $\bar{\gamma}_p \simeq \Gamma_{43}$ for $\epsilon_p \sim 1$. With the definitions of ϵ_e and ϵ_p , one has $\bar{\gamma}_e - 1 = (\epsilon_e n_p / \epsilon_p n_1)(m_p/m_e)(\bar{\gamma}_p - 1)$. The minimum Lorentz factors of electrons and protons can be written as $(\gamma_{e,m} - 1) = \phi(p)(\bar{\gamma}_e - 1)$, and $(\gamma_{p,m} - 1) = \phi(p)(\bar{\gamma}_p - 1)$, respectively, with $\phi(p) \simeq (p-2)/(p-1)$ for $p > 2$, and $\phi(p) = [\ln(\gamma_M/\gamma_m)]^{-1}$ for $p = 2$ (γ_M and γ_m are the maximum and minimum Lorentz factors of the power law distribution of the protons or electrons, respectively). Noticing $\hbar e B_q / m_e c = m_e c^2$, where $B_q = 4.414 \times 10^{13} \text{ G}$, one can finally express Eq.(5) into

$$E_{p,\text{IS}} \sim \frac{m_e c^2}{B_q} [\phi(p)]^2 \left(\frac{m_p}{m_e} \right)^2 \left(\frac{2L_\gamma}{R_{15}^2 c} \right)^{1/2} (1+z)^{-1}$$

$$\begin{aligned}
& \times \left[\left(\frac{\epsilon_B}{\epsilon_e} \right)^{1/2} \left(\frac{\epsilon_e n_p}{\epsilon_p n_e} \right)^2 (\bar{\gamma}_p - 1)^2 \right] \\
& \simeq 4.4 \text{ keV} \left[\frac{\phi(p)}{1/6} \right]^2 L_{\gamma,52}^{1/2} R_{\text{IS},14}^{-1} \left(\frac{1+z}{2} \right)^{-1} \\
& \times \left[\left(\frac{\epsilon_B}{\epsilon_e} \right)^{1/2} \left(\frac{\epsilon_e n_p}{\epsilon_p n_e} \right)^2 (\bar{\gamma}_p - 1)^2 \right]. \quad (8)
\end{aligned}$$

Since in internal shocks one expects $\epsilon_B \sim \epsilon_e^2 < \epsilon_e$ (Medvedev 2006), $\epsilon_e \ll \epsilon_p$, and $(\bar{\gamma}_p - 1) \sim 1$ (Eq.[7], unless a very large Γ_{fs} , and hence, Γ_{43} is invoked), the typical E_p predicted in the standard IS synchrotron emission model is about 2 orders of magnitude lower than the observed value. In order to invoke synchrotron radiation as the mechanism to power GRB prompt emission, one needs to make an additional assumption $n_p/n_e \gg 1$, i.e. only a small fraction of electrons are accelerated (Bykov & Mészáros 1996; Daigne and Mochkovitch 1998).

The requirement of a small fraction of accelerated electrons is also introduced in correctly calculating the synchrotron self-absorption frequency (ν_a) in the IS model. Shen and Zhang (2009) (see their Appendix for details) showed that in order to get a self-consistent ν_a using two independent methods (one derived from the blackbody approximation in the self-absorbed regime and another derived from the standard approach of applying electron energy distribution (Rybicki and Lightman 1979), one generally requires that not all electrons associated with the baryonic ejecta are accelerated.

By modeling particle acceleration in relativistic shocks using particle-in-cell (PIC) simulations, Spitkovsky (2008) indeed showed that only a small fraction of electrons are accelerated, and that most electrons ($\sim 99\%$ in number and $\sim 90\%$ in energy) are distributed in a relativistic Maxwellian. The numerical simulation shows growth of the non-thermal tail with simulation time. Spitkovsky (2008) suspects that the thermal peak may eventually get “significantly eroded”. In any case, it would be interesting to investigate the observational evidence of the putative thermal bump. The prompt GRB spectrum is usually well fit by a Band function (e.g. Abdo et al. 2009), which does not show a thermal-like bump near E_p (which is believed to be related to the injection energy of electrons due to the fast cooling argument presented in Sect.2.1.3). This suggests that the putative thermal bump may not be significant (if it exists at all) in the internal shocks within the IS model. Giannios and Spitkovsky (2009) interpret the early X-ray afterglow steep decay phase with significant spectral evolution (Zhang et al. 2007) as due to sweeping of the thermal bump across the X-ray band. This interpretation inevitably attributes the emission phase before the steep decay phase also to the external shock origin. Observationally it is established that the X-ray steep decay phase is a natural extension of the prompt emission (Tagliaferri et al. 2005; Barthelmy et al. 2005; O’Brien et al. 2006). The erratic temporal behavior of the prompt emission is difficult to be accounted for within the same external shock model that interprets the X-ray afterglow. A more natural interpretation would be that the steep decay is the high-latitude emission of the prompt emission as long as the instantaneous spectrum

at the end of the prompt emission phase is characterized by a “curved” spectrum instead of a simple power law (Zhang et al. 2009a).

2.1.5. The Amati/Yonetoku relation inconsistency

Observationally, more energetic GRBs tend to be harder. This is manifested as the correlations $E_p \propto E_{\gamma,iso}^{1/2}$ (Amati et al. 2002) and $E_p \propto L_{\gamma}^{1/2}$ (Wei and Gao 2003; Yonetoku et al. 2004) with large scatter. The relations are also found to apply for different emission episodes within the same burst (Liang et al. 2004; Ghirlanda et al. 2009)⁷. Inspecting Eq.(8), interpreting this correlation within the IS synchrotron emission model requires that R_{14} does not vary significantly among bursts, i.e. the internal shock radius is insensitive to the GRB luminosity. Inspecting Eq.(2), this suggests that GRBs all share a similar Lorentz factor regardless of their luminosities (Zhang and Mészáros 2002a). Furthermore, increasing the average Γ (and hence Γ_s) tends to make a GRB softer (a larger R_{14}), this is in contrast to the naive expectation that high- Γ GRBs tend to be harder. Recently, Liang et al. (2010) discovered a tight correlation between Γ and $E_{\gamma,iso}$ based on the deceleration signature of a sample of GRBs with known redshift, namely $\Gamma \propto E_{\gamma,iso}^{0.27}$. Taking the trivial proportionality of $L_{\gamma} \propto E_{\gamma,iso}$, this gives $R_{\text{IS}} \propto \Gamma^2 \propto L_{\gamma}^{0.54}$ and $E_p \propto E_{\gamma,iso}^{-0.04}$ (Liang et al. 2010), which is far from the observed Amati relation. This is another difficulty of the IS model.

2.1.6. The missing bright photosphere problem

In order to develop strong internal shocks, the composition of the GRB ejecta has to be baryonic, i.e. $\sigma \ll 1$. Such a baryonic outflow is believed to be accelerated from a fireball that initially carries most of its energy in thermal form and converts this energy to kinetic form during the acceleration process (Paczýnski 1986; Goodman 1986; Shemi and Piran 1990). As the fireball becomes transparent, a bright thermal emission component is expected to leak out from the fireball photosphere, which forms a distinct thermal emission component in the GRB spectrum. Such a thermal component is predicted bright enough to be usually detectable along with the IS non-thermal emission component (Mészáros and Rees 2000; Mészáros et al. 2002; Pe’er 2008). In the past, since the detector bandpass (e.g. for BATSE and Swift BAT) was not wide enough, there have been several speculations regarding this thermal component. The two leading possibilities are: (1) the observed Band-function is the non-thermal component powered by internal shocks, and the photosphere component is either below or above the detector energy band; (2) the observed Band function is the superposition of a thermal component and a non-thermal component (Ryde 2005; Ryde and Pe’er 2009). The excellent observational data of GRB 080916C with Fermi (thanks to the broad band coverage of Fermi GBM and LAT) show no evidence of deviation of the Band-

⁷ Some arguments have been raised to show that the global Amati relation is a pure observational selection effect (Nakar and Piran 2005; Band and Preece 2005; Butler et al. 2007), but the fact that the correlation also exists internally in individual GRBs suggest a physical link between E_p and L_{γ} .

function spectrum both below and above E_p . This immediately rules out these possibilities (1) and (2). If one accepts that the observed non-thermal emission from GRB 080916C is the emission from the internal shock, a profound question would be “where is the thermal component?”. In fact, using the observed minimum variability time scale revealed by the GRB 080916C data, the predicted photosphere thermal emission component is more than one order of magnitude brighter than the observed flux. This raises a severe problem to the fireball acceleration scenario and the straightforward IS model (Zhang and Pe’er 2009). This is the “missing bright photosphere” problem of the IS model.

A plausible scenario is to interpret the entire Band spectrum as the emission from the photosphere. This requires energy dissipation below and above the photosphere (defined by Thomson scattering optical depth being unity). This model is discussed in detail in Sect.2.3 below.

2.1.7. Other variants of the IS model

There are two variants of the IS model that invoke different radiation mechanisms other than synchrotron emission. These variants all suffer from the same efficiency and fast cooling problems, but may introduce extra ingredients to confront other problems/issues discussed above. The first one is to invoke synchrotron self-Compton (SSC) as the mechanism for GRBs (Panaitescu and Mészáros 2000; Kumar and Panaitescu 2008; Racusin et al. 2008; Kumar and Narayan 2009). The allowed parameter space for SSC is larger than synchrotron to interpret the GRB data (Kumar and McMahon 2008). However, the SSC model suffers from the following drawbacks. First, it generally predicts a bright prompt optical emission component. Although this is consistent with GRB 080319B (Racusin et al. 2008), prompt optical emission data of other GRBs are generally consistent with the extrapolation of the gamma-ray spectrum to the optical band (Shen and Zhang 2009). Second, a dominant SSC component inevitably predicts higher order SSC components, which greatly increases the energy budget of GRBs (Derishev et al. 2001; Kobayashi et al. 2007; Piran et al. 2009). Third, the synchrotron/SSC model may not reproduce the much more variable gamma-ray light curve (than the optical light curve) observed in GRB 080319B (Resmi & Zhang 2010). Finally, E_p in the SSC model very sensitively depends on the Lorentz factor of the electrons ($E_p \propto \gamma_{e,p}^4$), so that a small dispersion of the $\gamma_{e,p}$ distribution gives a very wide range of E_p distribution (Zhang and Mészáros 2002a). This makes the parameters more contrived to account for the observed narrow clustering of E_p for bright BATSE GRBs (Preece et al. 2000).

Another IS model variant is to invoke “jitter” emission as the radiation mechanism (Medvedev 2000). In this scenario, the magnetic field in the emission region has a random configuration, with a coherent length scale $\lambda_B \ll R_B = \gamma_e m_e c^2 / eB'$, the Larmor radius. Electrons in such a field hardly make one gyration before the field direction changes. As a result, the typical frequency of the radiation spectrum is no longer related to the strength of the field, but is related to the coherent

length, i.e.

$$E_p \sim \hbar \Gamma \gamma_{e,p}^2 \frac{c}{\lambda_B} (1+z)^{-1}, \quad (9)$$

which is by definition much larger than E_p in the synchrotron emission model (Eq.[5]) given the same $\gamma_{e,p}$. This eases the constraint discussed in §2.1.4. However, since there is no prediction on λ_B from the first principle (and it is not clear whether such a characteristic scale exists), it is not easy to assess how E_p depends on model parameters. In particular, the correlation $E_p \propto L_\gamma^{1/2}$ established in the synchrotron model (Eq.[8]) is no longer straightforward to justify. Recently, Sironi and Spitkovsky (2009) synthesized the particle spectrum from PIC simulations and concluded that the spectrum is entirely consistent with synchrotron radiation in the magnetic fields generated by Weibel instability. The “jitter” regime is recovered only when one artificially reduces the strength of the electromagnetic fields.

2.2. The electromagnetic model

In another extreme, i.e. $\sigma \gg 1$, a so-called Electro-Magnetic model (EM model) (Lyutikov and Blandford 2003; Lyutikov 2006b) has been proposed. In the high- σ regime, the comoving Alfvén speed is close to speed of light, which can be written as (Jackson 1975)

$$V'_A = \frac{cV'_{A,\text{NR}}}{(c^2 + V'^2_{A,\text{NR}})^{1/2}}, \quad (10)$$

where

$$V'_{A,\text{NR}} = \frac{B'}{\sqrt{4\pi\rho'}} = \sqrt{\sigma c} \quad (11)$$

is the comoving Alfvén speed in the non-relativistic regime (noticing the definition of σ in Eq.[1]), one can write the Lorentz factor of the comoving Alfvén wave as

$$\gamma'_A = (1 + \sigma)^{1/2}. \quad (12)$$

For a cold plasma (i.e. the comoving thermal energy density much smaller than the rest mass energy density, and hence, the magnetic energy density), gas sound speed is much less than the Alfvén speed. Therefore γ'_A is also approximately the comoving Lorentz factor of other magnetoacoustic waves. The EM model (Lyutikov and Blandford 2003) applies to the “sub-Alfvénic” regime, i.e. $\Gamma < \gamma'_A = (1 + \sigma)^{1/2}$, or roughly

$$\sigma > \sigma_c \equiv \Gamma^2 - 1 \sim 10^6 \Gamma_3^2 \quad (13)$$

at the deceleration radius. According to this model, the Poynting flux is dissipated through electromagnetic current-driven instabilities. The model has some novel features that are not shared by the fireball IS model. For example, the emission radius where strong magnetic dissipation occurs is $R \sim 10^{16}$ cm, much larger than that of internal shocks defined by the minimum variability time scales (Eq.[2]). This large radius is consistent with independent constraints on GRB emission site using different methods (Lyutikov 2006a; Kumar et al. 2007; Shen and Zhang 2009; Gupta and Zhang 2008; Zhang and Pe’er 2009). The EM model also justifies a “structured” jet with energy per unit solid angle dropping with angle as $E(\theta) \propto \theta^{-2}$, as has been invoked

in some GRB phenomenological models (Mészáros et al. 1998; Rossi et al. 2002; Zhang and Mészáros 2002b).

There are however two major issues related to the EM model. The first one is regarding its extremely high- σ value at the deceleration radius. Lyutikov and Blandford (2003) argued a force-free flow by invoking $\sigma \sim 10^9$ beyond the photosphere. However, considering more realistic models to launch a magnetized outflow from the central engine would lead to a range of σ values that are below σ_c (e.g. Spruit et al. 2001). At the extreme, even the outflow consists of cold (pressureless) matter accelerated exclusively by the magnetic field, the achievable σ is at most σ_c (Michel 1969). Such a maximally magnetized outflow is achievable only at a specified geometry, i.e. a purely radially expanding outflow. For more general geometric configurations, the achievable σ should be below σ_c , and could be as low as $\sigma \leq 1$ (Begelman and Li 1994; Spruit et al. 2001). If one considers the “collapsar” scenario of long GRBs (Woosley 1993; MacFadyen and Woosley 1999), a PFD jet launched from the central engine needs to penetrate through the stellar envelope. The σ value would be further degraded. Recent numerical simulations (Tchekhovskoy et al. 2008; Nagataki 2009) suggest that a high- σ flow at the base of the flow would become a moderate- σ flow as it escapes the star (cf. Wheeler et al. 2000).

Another issue of the EM model is related to GRB variability time scales. According to the EM model, the GRB central engine is assumed to launch a magnetic bubble, which expands and exits the star without degrading σ , and magnetic energy is finally dissipated by the current-driven instability at a large radius $R \sim 10^{16}$ cm (Lyutikov and Blandford 2003). The observed rapid variability of the GRB light curves is interpreted as due to emission from some “fundamental emitters” that are moving relativistically with respect to the dissipation region, which itself is moving relativistically with respect to the observer. A related model invoking relativistic, possibly magnetic turbulence was recently proposed by Narayan and Kumar (2009) and Kumar and Narayan (2009). Within such a picture, the observed variability time scale does not reflect the behavior of the GRB central engine. As discussed earlier in §2.1, the connection between at least the slow variability time scales with GRB central engine activity is strongly supported by the data (Liang et al. 2006), especially in view of the discovery of X-ray flares that extend central engine activity to later times (Burrows et al. 2005; Chincarini et al. 2007; Falcone et al. 2007). Attributing the observed variability to random motion of the relativistic “fundamental emitters” in the emission region (Lyutikov and Blandford 2003) would then require arguing that the “ T_0 -reset” effect of the last pulse and X-ray flares (Liang et al. 2006) is purely due to a chance coincidence.

2.3. MHD and dissipative photosphere models

If the magnetized ejecta can be approximated as a fluid and described by magnetohydrodynamics (MHD) (Spruit et al. 2001), the GRB models are in the MHD

regime⁸. Within this regime, outflows launched from the central engine would carry a dynamically important magnetic field, but it can be still approximated as a MHD fluid⁹. The σ value may decrease with increasing radius due to two mechanisms. First, below the photosphere, reconnection dissipation energy is thermalized in the plasma because of the high optical depth of the radiated photons. The thermal energy is then converted to bulk kinetic energy similar to the fireball acceleration process (Drenkhahn 2002; Drenkhahn and Spruit 2002). This scenario is more relevant to the so-called “striped wind” magnetic field configuration with alternating magnetic polarity (relevant to pulsar-like central engine with misaligned magnetic and rotational axes). For helical magnetic configurations (relevant to black hole central engine with rotational and magnetic axes aligned), the neighboring ordered field lines typically have the same orientation, so that reconnection is greatly suppressed. Second, the Poynting flux may be directly converted to kinetic energy without dissipation (e.g. Vlahakis and Königl 2003; Komissarov et al. 2009) under the pressure gradient of magnetic fields in an MHD flow. The efficiency of such a conversion is, however, subject to uncertainties. Without an external pressure confinement, the Poynting flux energy cannot be fully converted to kinetic energy, and the flow can be only accelerated up to $\Gamma_{\text{tot}}^{1/3}$, where Γ_{tot} is the Lorentz factor for total conversion (Beskin et al. 1998). This was the origin of the well known “ σ problem” of the Crab nebula. The jet acceleration can be efficient with an external confinement, which is relevant to GRBs in the collapsar scenario (e.g. Tchekhovskoy et al. 2008). In any case, the pressure gradient has to be small enough for efficient acceleration to happen (Lyubarsky 2010). Overall, if the jet has $\sigma_0 \gg 1$ at the central engine, the σ value at the GRB emission region can range from $\sigma \leq 1$ to $\sigma \leq \sigma_0$, depending upon how efficient the conversion from Poynting flux to kinetic flux would be. Lyubarsky (2010) showed that it is difficult to have a completely matter dominated jet (say, $\sigma < 0.1$) at the GRB emission radius for a dissipation-less jet with an initial high σ , even if the most efficient conversion occurs (see also Levinson 2010).

⁸ Lyutikov (2006b) defines this regime as $1 < \sigma < \sigma_c \equiv \Gamma^2 - 1 \sim 10^6 \Gamma_3^2$, opposed to the sub-Alfvénic regime invoked by the EM model. He also relates the “super-Alfvénic” and “sub-Alfvénic” regimes to whether or not a shock can exist in the ejecta. Such a connection is relevant only for 1D ejecta-medium interaction. A more relevant condition to discuss shock formation condition in the high- σ regime is whether the magnetized ejecta encounters a stronger pressure than its own magnetic pressure (Zhang and Kobayashi 2005; Mizuno et al. 2009a). For collisions between two shells with the same σ value, internal shocks can develop even for a small relative Lorentz factor between the two shells. For an expanding shell with small width (thin shell) and conical geometry, the reverse shock cannot form for $\sigma > (10 - 100)$ (Zhang and Kobayashi 2005).

⁹ Strictly speaking, the outflow may not satisfy the MHD condition at all radii. Since the particle density $n \propto R^{-2}$ decays with radius faster than the Goldreich-Julian density $n_{\text{GJ}} \propto R^{-1}$, the MHD condition would break above a critical radius R_{MHD} . If this radius is beyond the deceleration radius ($R_{\text{MHD}} > R_{\text{dec}}$) (Spruit et al. 2001), then the MHD condition would not break before afterglow sets in. However, if $R_{\text{MHD}} < R_{\text{dec}}$, the MHD condition breaks at R_{MHD} and a strong magnetic dissipation occurs between R_{MHD} and R_{dec} . This happens if σ is larger than a few hundred (Zhang and Mészáros 2002a). We do not discuss this regime in this paper by limiting our discussion to the regime of $1 \lesssim \sigma \lesssim 100$.

In the past, the GRB prompt emission models in the MHD regime (Spruit et al. 2001; Drenkhahn 2002; Drenkhahn and Spruit 2002; Vlahakis and Königl 2003; Giannios 2008) have been “semi-fireball” like. It is generally assumed that an initial high σ is reduced to $\sigma < 1$ before the jet reaches the internal shock radius, so that the traditional IS model can still apply at R_{IS} . Such a model shares essentially the same advantages and drawbacks of the IS model. The data of GRB 080916C give a strong constraint on such a model: the lack of a photosphere component requires that either $\sigma \gg 1$ at the photosphere, or $\sigma < 1$ already at the photosphere. For the former, the magnetic-to-kinetic energy transition efficiency is low. One cannot have matter-dominated internal shocks. For the latter, the magnetic acceleration proceeds in a “cold” and efficient way, which is difficult to achieve theoretically. The external confinement of the high- σ flow (which is required for efficient magnetic acceleration) would inevitably cause heating of the jet to result in a bright photosphere, which is constrained by the data of GRB 080916C. Even if the flow could become baryon-dominated through magnetic acceleration without a hot photosphere component, the internal shock efficiency is so low that only a small fraction of energy (say $\sim 10\%$) is converted to gamma-ray radiation. This greatly increases the total energy budget of the outflow, and demands an even higher σ at the central engine to begin with (from the missing bright photosphere argument). This makes it even more difficult to efficiently convert Poynting flux energy to kinetic energy.

A plausible scenario is to argue that the observed spectrum is dominated by the emission from the photosphere itself, and that the internal shock emission is too weak to be detected. Within such a scenario, there is no “missing photosphere” problem, since the observed spectrum is the photosphere emission itself. One then needs to argue that the entire non-thermal GRB spectrum is the reprocessed photosphere thermal emission. This requires significant energy dissipation below and above the photosphere (Thompson 1994; Rees and Mészáros 2005; Thompson 2006; Thompson et al. 2007; Ghisellini et al. 2007; Giannios 2008; Beloborodov 2010; Lazzati and Begelman 2010). Within the MHD models, the dissipation source is continuous magnetic reconnection (for the striped-wind geometry). Such a model can be also developed for a neutron-rich baryonic flow with $\sigma \ll 1$, in which neutron decay provides a source of continuous heating in the jet (Beloborodov 2010). By properly considering Compton upscattering of photosphere thermal photons, a hard power law tail can be produced (Beloborodov 2010; Lazzati and Begelman 2010). This model can also naturally interpret GRB variability in terms of the central engine energy injection history. The radiative efficiency is also naturally high (Lazzati et al. 2009). Confronting the GRB 080916C data, however, this model faces two difficulties.

First, the maximum photon energy in the dissipative photosphere model is $\sim 0.1 - 1$ GeV (Beloborodov 2010; Lazzati and Begelman 2010). The detection of 13.2 GeV photon associated with one of the GBM pulses in GRB 080916C (which corresponds to 70.6 GeV rest-frame) then disfavors the photosphere origin of gamma-ray emission in GRB 080916C. It has been argued that the GeV

emission of LAT GRBs including GRB 080916C may be of the external shock origin (Kumar and Barniol Duran 2009; Ghisellini et al. 2010). However, the required forward shock parameters are extreme, which are not easy to accommodate within the known relativistic shock models (Kumar and Barniol Duran 2010; Li 2010b; Piran and Nakar 2010). Furthermore, the LAT-band emission and GBM-band emission generally trace each other during the prompt emission phase (Zhang et al. 2010)¹⁰. For GRB 080916C, the time-resolved spectral analysis with the finest temporal resolution defined by statistics suggests that the Band function fits well the data for every time bin throughout the burst. The peak of the GeV emission in the logarithmic light curve coincides with the second peak of the GBM light curve. All these strongly suggest that the entire emission of GRB 080916C is from the same emission region, and is therefore likely of an internal origin (see Zhang et al. 2010 for more detailed discussion). The long term GeV emission, on the other hand, decays slower than the MeV emission. It may be dominated by a different emission component (e.g. external shock).

Second, although the high energy photon spectral index above E_p can be well reproduced in the dissipative photosphere model by Compton upscattering (Beloborodov 2010; Lazzati and Begelman 2010), the low energy photon spectral index below E_p is typically much harder than what is observed. For up-Comptonization of a blackbody spectrum (e.g. within the context of soft gamma-ray repeaters and anomalous X-ray pulsars), the Rayleigh-Jeans low energy spectral index (Band-function index $\alpha = +1$) is hardly affected (Nobili et al. 2008). By invoking dissipation below the photosphere (e.g. neutron heating), this index can be modified to $\alpha = +0.4$ (Beloborodov 2010), still much harder than the observed typical value $\alpha \sim -1$ (Abdo et al. 2009; Zhang et al. 2010). One possibility would be to assume that the observed low energy spectrum is the superposition of the photosphere emission of many shells (e.g. Toma et al. 2009, 2010). Although this is not impossible, it requires properly arranging the luminosity and Lorentz factor of many mini-shells to mimic a typical $\alpha = -1$ Band spectrum. A detailed time-resolved spectral analysis of GRB 080916C and other “Band-only” GRBs suggests that the low energy photon index α remains essentially unchanged as the time bin becomes progressively small (Zhang et al. 2010). This at least disfavors the possibility that the observed time-integrated spectrum is the temporal superposition of the photosphere emission of many shells. One plausible solution would be to introduce synchrotron and synchrotron self-Compton (SSC) of the electrons. In the MHD model, if continuous magnetic heating is operating, the SSC component would produce a typical Band spectrum in the MeV range, if most energy dissipation happens in the Thomson-thin region above the photosphere (e.g. Fig. 2 of Giannios 2008). Such a model predicts a bright optical emission component (synchrotron). Although this is consistent with the case of GRB 080319B (Racusin et al. 2008), it is inconsistent with most of the prompt optical emission data or upper limits, which are consistent with

¹⁰ This is the case even for GRB 090902B, which clearly shows two distinct spectral components.

or below the extrapolation of gamma-ray spectrum to the optical band (Shen and Zhang 2009).

2.4. Summary

In summary, the new Fermi LAT data of GRB 080916C raises a challenge to the traditional fireball IS model, which has some advantages and drawbacks. The EM model invokes too high a σ at the deceleration radius, which may not be achieved in nature. We consider the moderate- σ MHD regime a relevant regime for GRB outflows. However, the current semi-fireball MHD models or the dissipative photosphere models are not ideal to adequately interpret GRB 080916C. The ICMART model proposed in this paper is meant to inherit the merits of the existing models and to overcome their drawbacks.

Since most LAT GRBs are found similar to GRB 080916C to show “Band-only” time-resolved spectra (Zhang et al. 2010), we argue that the proposed model would be relevant to most GRBs.

3. THE ICMART MODEL

3.1. Basic assumptions

The Internal-Collision-induced MAGnetic Reconnection and Turbulence (ICMART) model is based on the following two assumptions:

1. The GRB central engine is intermittent in nature, which ejects an unsteady outflow with variable Lorentz factors and luminosities but a nearly constant degree of magnetization. Approximating the unsteady outflow as some discrete shells with variable Lorentz factors, these magnetized shells collide with each other at the conventional internal shock radius R_{IS} (Eq.[2]).
2. The GRB central engine is highly magnetized, which ejects a high- σ flow from the base of the central engine. Although various mechanisms (e.g. magnetic acceleration and reconnection) may reduce σ as the outflow streams outwards, the ejecta is still moderately magnetized in the GRB emission region, with σ ranging from $1 < \sigma \lesssim 100$.

In an ideal magnetically driven MHD jet, magnetic energy is converted into kinetic energy during the expansion. Usually it is assumed that $\sigma_0 \gg 1$ at the central engine with $\Gamma_0 \sim 1$. The magnetization parameter σ then decreases with radius as Γ increases with radius (Beskin et al 1998; Vlahakis and Königl 2003; Komissarov et al. 2009; Lyubarsky 2010; Granot et al. 2010). Without external pressure confinement, the early acceleration phase reaches a Lorentz factor $\Gamma \sim \sigma_0^{1/3}$, with remaining magnetization $\sigma \sim \sigma_0^{2/3}$. Beyond this radius acceleration is slow and weakly dependent on R , e.g. $\Gamma \propto R^{1/3}$, and $\sigma \propto R^{-1/3}$ (Granot et al. 2010). If σ_0 remains roughly constant, one expects a nearly constant σ at large radii, but in the meantime does not expect a large variation in Γ . We note, however, that near the rapidly-rotating magnetized central engine, efficient acceleration of ejecta may occur below the light cylinder thanks to direct electric field accelerate mechanisms (e.g. frame-dragging-induced deviation from the force-free condition, Muslimov & Tsygan 1992 within the

context of pulsars). As a result, at the light cylinder (effectively the base of central engine), the ejecta may have $\Gamma_0 \gg 1$. The rapid variation of the jet power (e.g. due to variable accretion rate or variable spindown rate of the central object) may lead to a variable Γ and somewhat variable σ_0 at the central engine. Considering later magnetic acceleration, one may get a large Γ variation within the outflow, with σ not significantly varying at a same radius. Our above two assumptions may be then fulfilled.

3.2. Basic parameters of the GRB ejecta plasma

In preparation of proposing the model, it is informative to summarize the basic parameters of GRB ejecta. The gamma-ray emission radius R can be in principle in the range of $10^{11} - 10^{17}$ cm (bracketed by the photosphere radius and the external shock deceleration radius). As will become evident later, several collisions are needed to trigger an ICMART event, so that one would have $R_{\text{ICMART}} \geq R_{\text{IS}}$. In the following, in order to make differentiation with the IS model, we will normalize all radii relevant for the ICMART model to $R = 10^{15}$ cm R_{15} , and denote R as R_{ICMART} whenever relevant.

1. *Length scales:* At R_{ICMART} , the “thickness” of the ejecta is related to the radius R^{11} , i.e.

$$\Delta' = \frac{R}{\Gamma} \simeq 3.2 \times 10^{12} \text{ cm} R_{15} \Gamma_{2.5}^{-1} \quad (14)$$

in the comoving frame, and

$$\Delta = \frac{R}{\Gamma^2} \simeq 10^{10} \text{ cm} R_{15} \Gamma_{2.5}^{-2} \quad (15)$$

in the rest frame of the central engine (lab frame). Assuming a conical jet with the opening angle θ_j , the cross section radius of the emission region is

$$R_\theta = R\theta_j = 8.7 \times 10^{13} \left(\frac{\theta_j}{5^\circ}\right) R_{15} \text{ cm} \quad (16)$$

in both the lab frame and the comoving frame. Typically one has $R_\theta \gg \Delta' \gg \Delta$. GRB ejecta are therefore also considered as “flying pancakes”.

2. *Plasma number density:* In a conical jet, density drops with radius as R^{-2} . For a hydrogen ejecta with a total “wind” luminosity L_w , Lorentz factor Γ , and magnetization parameter σ , the comoving ejecta proton number density is

$$n'_p = \frac{L_w}{4\pi(1+\sigma)R^2\Gamma^2(m_p + Ym_e)c^3} \\ \simeq 1.8 \times 10^7 \text{ cm}^{-3} L_{w,52} \Gamma_{2.5}^{-2} R_{15}^{-2} m^{-1} (1+\sigma)_1^{-1} \quad (17)$$

where $m = 1 + Ym_e/m_p \sim 1$ if the lepton (pair) multiplicity parameter $Y \ll m_p/m_e$. In the rest frame of the central engine, the ejecta proton number density is

$$n_p = \Gamma n'_p \simeq 5.6 \times 10^9 \text{ cm}^{-3} L_{w,52} \Gamma_{2.5}^{-1} R_{15}^{-2} m^{-1} (1+\sigma)_1^{-1}. \quad (18)$$

¹¹ This approximation is based on the assumption of shell-spreading. For high- σ shells, the spreading condition may be more stringent (Granot et al. 2010). The shell width is then related to the duration of the central engine, not a function of R . In any case, the following estimates are valid to order of magnitude.

The electron number (or more generally the lepton number) densities are

$$n'_e = Y n'_p, \quad n_e = Y n_p. \quad (19)$$

3. *Magnetic field strength:* The comoving magnetic field strength is

$$B' = \left(\frac{L_w}{\Gamma^2 R^2 c} \frac{\sigma}{1 + \sigma} \right)^{1/2} \\ \simeq 1.8 \times 10^3 \text{ G} \left(\frac{\sigma}{1 + \sigma} \right)^{1/2} L_{w,52}^{1/2} \Gamma_{2.5}^{-1} R_{15}^{-1}. \quad (20)$$

In the lab frame, the magnetic field strength is

$$B = \Gamma B' \simeq 5.8 \times 10^5 \text{ G} \left(\frac{\sigma}{1 + \sigma} \right)^{1/2} L_{w,52}^{1/2} R_{15}^{-1}. \quad (21)$$

This \mathbf{B} field is accompanied by an induced $\mathbf{E} = -\mathbf{V} \times \mathbf{B}$ field for an ideal MHD fluid.

4. *Collisional mean free path and time scale:* For Coulomb collisions, the strong collision radius can be defined by $e^2/r_{col} \sim kT$ so that $r_{col} \sim e^2/kT \sim (1.7 \times 10^{-3} \text{ cm})/T$. Here kT denotes more generally the typical energy of the particles (which are not necessarily in thermal equilibrium). The comoving collision mean free path of electrons can then be estimated as

$$l'_{e,col} = (n'_e \pi r_{col}^2)^{-1} \simeq 6.5 \times 10^{17} \text{ cm} \\ \times L_{w,52}^{-1} \Gamma_{2.5}^2 R_{15}^2 m Y^{-1} (1 + \sigma)_1 T_{e,10}^2. \quad (22)$$

In order to have the plasma in the ‘‘collisional’’ regime, one needs to require $l'_{e,col} < \Delta'$. This is translated into $T_e < T_{e,c} \equiv 2.2 \times 10^7 \text{ K} L_{w,52}^{1/2} \Gamma_{2.5}^{-3/2} R_{15}^{-1/2} m^{-1/2} Y^{1/2} (1 + \sigma)_1^{-1/2}$. Downstream of the GRB internal shocks, the effective proton temperature is of the order of $T_p \sim (\Gamma_{ud} - 1) m_p c^2 / k \sim 1.1 \times 10^{13} \text{ K} (\Gamma_{ud} - 1)$ (where Γ_{ud} is the relative Lorentz factor between upstream and downstream), and the electron temperature is even higher by a factor of $(\epsilon_e / \epsilon_p) (m_p / m_e)$. As a result, GRB shocks must be ‘‘collisionless’’. In the upstream, the temperature can be lower, but since the flow is relativistic, any inhomogeneity in the velocity field would result in ‘‘heating’’ in the flow. Other processes (magnetic reconnection, neutron decay, etc) would also enhance heating, so that the electron temperature may be maintained to be significantly above $T_{e,c}$. For a reasonable estimate, the electrons in a relativistic flow would have at least a relativistic temperature $T_e \sim m_e c^2 / k = 5.9 \times 10^9 \text{ K}$. The collision time scale can be estimated as $\tau'_{col} = l'_{e,col} / v'_e$. For a non-relativistic temperature, one has $v'_e = (2kT_e / m_e)^{1/2}$, so that the comoving collision time $\tau'_{col, NR} = m_e^{1/2} (kT_e)^{3/2} / (\sqrt{2} \pi e^4 n'_e)$. In the GRB ejecta (even without shock heating), it is very possible that the electrons have a comoving relativistic temperature, so that $v'_e \sim c$. The comoving collisional time is therefore

$$\tau'_{col,R} = \frac{l'_{e,col}}{c} \simeq 2.2 \times 10^7 \text{ s} \\ \times L_{w,52}^{-1} \Gamma_{2.5}^2 R_{15}^2 m Y^{-1} (1 + \sigma)_1 T_{e,10}^2, \quad (23)$$

which is $\gg t'_{dyn} = R/\Gamma c \sim 110 \text{ s} R_{15} \Gamma_{2.5}^{-1}$, the comoving dynamical time scale. This again suggests that ejecta is collisionless even without strong shock heating.

5. *Gyroradii and gyrofrequencies:* Another relevant length scale is the particle gyro-radius in magnetic fields. Without direct collisions, the GRB ejecta can be still approximately described as a ‘‘fluid’’ macroscopically. This is because particles are interacting with each other through magnetic fields microscopically. Fundamentally the smallest length scale is defined by particle gyration. The comoving frame gyro(cyclotron)-radii are

$$r'_{B,e} = \frac{\gamma_e m_e c^2}{e B'} \simeq 0.93 \text{ cm} \gamma_e L_{w,52}^{-1/2} \Gamma_{2.5} R_{15} \left(\frac{1 + \sigma}{\sigma} \right)^{1/2} \quad (24)$$

for electrons (where γ_e is the electron Lorentz factor), and

$$r'_{B,p} = \frac{\gamma_p m_p c^2}{e B'} \simeq 1.7 \times 10^3 \text{ cm} \gamma_p L_{w,52}^{-1/2} \Gamma_{2.5} R_{15} \left(\frac{1 + \sigma}{\sigma} \right)^{1/2} \quad (25)$$

for protons (where γ_p is the proton Lorentz factor). Given the typical γ_e values to interpret the GRB emission (Eq.[6]) and the related γ_p (which is typically smaller by a factor of $\epsilon_p m_e / \epsilon_e m_p$), both radii are $\ll \Delta'$. If the typical viscous length scale is not much larger than the gyration radius, the fluid description of the GRB plasma is justified. The comoving gyrofrequencies are

$$\omega'_{B,e} = \frac{e B'}{m_e c} \simeq 3.2 \times 10^{10} \text{ s}^{-1} L_{w,52}^{1/2} \Gamma_{2.5}^{-1} R_{15}^{-1} \left(\frac{\sigma}{1 + \sigma} \right)^{1/2} \quad (26)$$

for electrons, and

$$\omega'_{B,p} = \frac{e B'}{m_p c} = \omega'_{B,e} \frac{m_e}{m_p} \\ \simeq 1.7 \times 10^7 \text{ s}^{-1} L_{w,52}^{1/2} \Gamma_{2.5}^{-1} R_{15}^{-1} \left(\frac{\sigma}{1 + \sigma} \right)^{1/2} \quad (27)$$

for protons. Both are much larger than the inverse of the comoving dynamical time, i.e. $(R/\Gamma c)^{-1} \sim 9.5 \times 10^{-3} \text{ s}^{-1} \Gamma_{2.5} R_{15}^{-1}$, again justifying the fluid description.

6. *Plasma frequencies and plasma skin depths:* The comoving relativistic plasma frequencies are

$$\omega'_{p,e} = \left(\frac{4\pi n'_e e^2}{\bar{\gamma}_e m_e} \right)^{1/2} \simeq 2.4 \times 10^8 \text{ s}^{-1} \\ \times \bar{\gamma}_e^{-1/2} Y^{1/2} L_{w,52}^{1/2} \Gamma_{2.5}^{-1} R_{15}^{-1} m^{-1/2} (1 + \sigma)_1^{-1/2} \quad (28)$$

for electrons, and

$$\omega'_{p,p} = \left(\frac{4\pi n'_p e^2}{\bar{\gamma}_p m_p} \right)^{1/2} \simeq 5.5 \times 10^6 \text{ s}^{-1} \\ \times \bar{\gamma}_p^{-1/2} L_{w,52}^{1/2} \Gamma_{2.5}^{-1} R_{15}^{-1} m^{-1/2} (1 + \sigma)_1^{-1/2} \quad (29)$$

for protons. Here $\bar{\gamma}_e$ and $\bar{\gamma}_p$ denote the mean Lorentz factor of the relativistic electron and proton gas, respectively. The corresponding plasma

skin depths are

$$\delta'_e = \frac{c}{\omega'_{p,e}} \simeq 130 \text{ cm } \bar{\gamma}_e^{1/2} Y^{-1/2} L_{w,52}^{-1/2} \Gamma_{2.5} R_{15} m^{1/2} (1+\sigma)_1^{1/2} \quad (30)$$

for electrons, and

$$\delta'_p = \frac{c}{\omega'_{p,p}} \simeq 5.4 \times 10^3 \text{ cm } \bar{\gamma}_p^{1/2} L_{w,52}^{-1/2} \Gamma_{2.5} R_{15} m^{1/2} (1+\sigma)_1^{1/2} \quad (31)$$

for protons. Physically these quantities are relevant to a weakly magnetized ejecta with random B fields ($\sigma \ll 1$). For a $\sigma > 1$ flow with ordered magnetic fields, the plasma oscillation frequencies and skin depths are relevant only in the direction parallel to the magnetic field lines. In the perpendicular direction, the gyrofrequencies and gyroradii are more relevant.

3.3. Turbulent nature of the GRB ejecta

Turbulence is believed to be ubiquitous in astrophysical systems. This is because the Reynold's number, the ratio between the viscous diffusion time $\tau_\nu = L^2/\nu$ and the relative flow time scale $\tau_f = L/\delta V$,

$$R_e \equiv \frac{L\delta V}{\nu}, \quad (32)$$

is $\gg 1$ (mostly because of the large L involved in astrophysical systems), where L and δV are the characteristic length and relative velocity of the flow, and

$$\nu \sim c_s l \quad (33)$$

is the kinematic viscosity as defined in the MHD equation of motion

$$\rho \left(\frac{\partial \mathbf{V}}{\partial t} + \mathbf{V} \cdot \nabla \mathbf{V} \right) = -\nabla P + \mathbf{J} \times \mathbf{B} + \rho \nu \nabla^2 \mathbf{V}, \quad (34)$$

c_s is sound speed, and l is the mean free path of microscopic interactions that define the viscosity.

Since shear motion tends to distort the fluid while the viscous term tends to smear the distortion of the fluid, the flow would become highly distorted and turbulent when the Reynold's number is $\gg 1$.

Being magnetically dominated, most kinetic motions are concentrated in the direction perpendicular to the magnetic field. The corresponding perpendicular viscosity is (Spitzer 1962)

$$\nu_\perp = 1.7 \times 10^{-2} \text{ cm}^2 \text{ s}^{-1} n \ln \Lambda / (\sqrt{T} B^2), \quad (35)$$

where $\ln \Lambda$ is the Coulomb logarithm. $\Lambda = 3/2 e^3 \sqrt{k^3 T^3} / \pi n \min(1, \sqrt{4.2 \times 10^5 / T})$. For typical parameters adopted in this paper, one has $\nu_\perp \sim 3.7 \times 10^{-4} \text{ cm}^2 \text{ s}^{-1} \ll L\delta V \sim 10^{24} \text{ cm}^2 \text{ s}^{-1}$, so that $R_e \sim 10^{28} \gg 1$. Therefore the GRB ejecta is turbulent in nature. In the low- σ case, Zhang et al. (2009b) has shown numerically that the GRB ejecta with a mildly relativistic relative motion (relevant to internal shocks and late external shock in the trans-relativistic regime) quickly turns turbulent if a Kelvin-Helmholtz instability is triggered. In the high- σ regime, due to the strong magnetic pressure in the ordered magnetic fields, the condition to trigger turbulence would be more demanding (see §3.5). In any case, strong anisotropic turbulence can develop once the triggering condition is satisfied.

For a resistive magnetized flow, another relevant dimensionless parameter is the magnetic Reynold's number, the ratio between the magnetic resistive diffusion time $\tau_{dif} = L^2/\eta$ and the flow time $\tau_f = L/\delta V$,

$$R_m \equiv \frac{L\delta V}{\eta}, \quad (36)$$

where η is the magnetic diffusion coefficient, which is defined in the diffusive MHD induction equation

$$\frac{\partial \mathbf{B}}{\partial t} = \nabla \times (\mathbf{V} \times \mathbf{B}) + \eta \nabla^2 \mathbf{B}. \quad (37)$$

For the reason described above, we adopt the perpendicular resistivity in a strong magnetic field (Spitzer 1962),

$$\eta_\perp = 1.3 \times 10^{13} \text{ cm}^2 \text{ s}^{-1} \frac{Z \ln \Lambda}{T^{3/2}}. \quad (38)$$

For the typical parameters adopted in this paper, one has $\eta_\perp \sim 1 \text{ cm}^2 \text{ s}^{-1}$. This gives a huge R_m number, $R_m \sim 10^{24}$. The maximum resistivity is the ‘‘Bohm’’ diffusion, i.e.

$$\eta_B \lesssim r_B V \sim r'_{B,e} c. \quad (39)$$

This gives

$$R_{m,B} \simeq \Delta' / r'_{B,e} \simeq 3.4 \times 10^{12} \gamma_e^{-1} L_{w,52}^{1/2} \Gamma_{2.5}^{-2} \left(\frac{\sigma}{1+\sigma} \right)^{1/2}. \quad (40)$$

This is still a large value, suggesting that magnetic fields can be also highly distorted and turbulent if the turbulence triggering condition is satisfied.

Unlike the hydrodynamical turbulence that displays a Komolgorov solution, i.e. $dE(k) \propto k^{-5/3}$ (where k is the wave number and $E(k)$ is the energy per unit wave number), MHD turbulence is anisotropic and has different scaling in the directions perpendicular to and along the field line, namely $E(k_\perp) \propto k_\perp^{-5/3}$ (Komolgorov-type) and $E(k_\parallel) \propto k_\parallel^{-2}$ (Goldreich and Sridhar 1995; Cho et al. 2002). While the kinetic power in the turbulence drops with k quickly, the power of magnetic fields does not drop significantly with k . As a result, the ‘‘eddies’’ in smaller scales are even more stretched and appear elongated along the *local* magnetic field. The MHD turbulence in the $\sigma > 1$ regime is not well studied, but qualitatively it should be the natural extension of the physics in the low $\beta = P_{gas}/P_{mag}$ regime (Cho et al. 2002)¹². The main extension is that the relative motion must be relativistic in order to distort the magnetic field lines. This is not very demanding in a GRB, since the outflow itself is highly relativistic. The MHD turbulence in a GRB ejecta is relativistic in nature.

3.4. Magnetic reconnection in the GRB ejecta

Reconnection plays a fundamental role in both laboratory and astrophysical settings, although the full details of the process was not well understood until recently. The main difficulty was that in a steady state, the reconnection process proceeds very slowly (Sweet 1958; Parker

¹² Notice that β is not simply σ^{-1} , since P_{gas} is the thermal pressure of the gas, while in the definition of σ (Eq.[1]), the rest mass energy density is invoked. Even in the very low- β regime ($P_{gas} \sim 0$), the σ value can be still below unity.

1957), and is not adequate to account for the abrupt reconnection events observed in the lab and various astrophysical phenomena, such as solar flares. This was merely a theoretical problem as in reality reconnection is indeed fast since astrophysical magnetic fields would be completely entangled due to turbulent motions. In the standard non-relativistic Sweet-Parker scenario, two sets of field lines with opposite orientations approach each other and reconnect within a layer of thickness δ and length \mathcal{L} , which satisfy

$$\frac{\delta}{\mathcal{L}} = \frac{V_{in}}{V_A} = S^{-1/2}, \quad (41)$$

where the Lundquist number

$$S \equiv \frac{\mathcal{L}V_A}{\eta} \quad (42)$$

is essentially the magnetic Reynold's number in the Bohm diffusion approximation, with δV replaced by the Alfvén speed V_A , and L replaced by \mathcal{L} . Notice that for individual reconnection events, it can well be that $\mathcal{L} \ll L \sim R_\theta$ (Eq.[16]). In any case, S is usually a large number, so that the Sweet-Parker process is an extremely slow process, i.e. $V_{in} = V_A S^{-1/2} \ll V_A$. A fast steady-state reconnection scenario was proposed by Petschek (1964), which invokes a shorter width \mathcal{L} of the resistive layer. However, such a scenario is unstable unless the magnetic diffusion η increases near the X-point. Simulations with a constant η suggests that an initial Petschek configuration would quickly revert to the Sweet-Parker configuration (Uzdensky and Kulsrud 2000). Lazarian and Vishniac (1999) proposed that reconnections in magnetic fields with stochasticity can proceed rapidly, thanks to the turbulent nature of the magnetized fluid that both broadens the reconnection zone and allows many independent flux reconnection events to occur simultaneously. This turbulence model of 3D reconnection is confirmed by numerical simulations (Kowal et al. 2009), and is the basis of our discussion of the IC-MART model¹³.

In the presence of turbulence, a magnetic field reconnects over a local scale λ_\parallel rather than the global scale \mathcal{L} . This is the scale over which a magnetic field wanders away from its original direction by the thickness of the Ohmic diffusion layer. Accordingly, it is the parameter

$$s \equiv \frac{\lambda_\parallel V_A}{\eta} \quad (43)$$

rather than the Lundquist number S that matters. The comoving local reconnection rate is given by $V'_{\text{rec,loc}} \approx V_A s^{-1/2} \ll V_A \sim c$ (Lazarian and Vishniac 1999).

One may estimate the required global reconnection speed to power a GRB. For the high- σ flow invoked in this paper, a significant fraction of the magnetic field energy is converted into radiation. This requires that the dissipated magnetic energy in a shell with comoving width Δ' within the time scale $\Delta t'$ can power the observed gamma-ray luminosity, i.e. $\Gamma^2(B'^2/8\pi)4\pi R^2\Delta'/\Delta t' \sim 10^{52}L_{\gamma,52}$. To compare

against the definition of B' (Eq.[20]), this demands that the global reconnection speed

$$V'_{\text{rec,global}} = \frac{\Delta'}{\Delta t'} \sim \frac{L_{\gamma,52}}{L_{w,52}} \frac{1+\sigma}{\sigma} c \sim c. \quad (44)$$

In turbulent reconnection, the global reconnection rate is boosted from $V'_{\text{rec,loc}}$ by a factor of $\sim L/\lambda_\parallel$, since $\sim L/\lambda_\parallel$ field lines reconnect simultaneously (Lazarian and Vishniac 1999). As a result, the small local reconnection speed $V'_{\text{rec,loc}} \approx V_A s^{-1/2}$ is adequate to power a GRB if $(L/\lambda_\parallel)s^{-1/2} \geq 1$, or

$$\lambda_\parallel \leq L^{2/3} \left(\frac{\eta}{c}\right)^{1/3}. \quad (45)$$

For the Bohm diffusion limit (Eq.[39]), and taking $L \sim R_\theta$ (Eq.[16]), the condition for triggering a GRB by global turbulent reconnection can be written as

$$\lambda_\parallel \leq R_\theta^{2/3} r'_{B,e}{}^{1/3} \simeq 1.9 \times 10^9 \text{ cm} \\ \times \gamma_e^{1/3} \left(\frac{\theta_j}{5^\circ}\right)^{2/3} L_{w,52}^{-1/6} \Gamma_{2.5}^{1/3} R_{15} \left(\frac{1+\sigma}{\sigma}\right)^{1/6}. \quad (46)$$

This requires that the individual reconnection region length scale λ_\parallel is sufficiently small (e.g. much smaller than $R/\Gamma = 3.3 \times 10^{12} \text{ cm} R_{15} \Gamma_{2.5}^{-1}$, the typical ‘‘observable’’ scale due to relativistic beaming). This calls for multiple collision-induced perturbations to trigger turbulence as we discuss below.

3.5. Trigger of a reconnection-turbulence ‘‘avalanche’’ and the role of collision

We envisage internal interactions within the wind (i.e. collisions) as the main agent to induce turbulence. Similar to the IS picture, numerous collisions can occur within the wind. However, most collisions do not lead to a strong radiation signature. In the high- σ regime, strong shocks can still exist as long as the ram pressure received by a magnetized shell is higher than the rest-frame magnetic pressure (Zhang and Kobayashi 2005). However, if no significant magnetic energy dissipation occurs, the total released energy is at most $(1+\sigma)^{-1}$ of the total ejecta energy, even if all the baryonic energy is converted to heat and gets radiated away completely. This is the main reason that radiation efficiency is low without magnetic dissipation (Zhang and Kobayashi 2005).

In order to give rise to an efficient radiation episode, the collision must lead to an abrupt discharge of the magnetic field energy, so that the ending σ value is significantly smaller than the initial one, i.e. $\sigma_{\text{end}} \ll \sigma_{\text{ini}}$. This must be accompanied by an ‘‘avalanche’’ of magnetic reconnection/turbulence events. A critical condition to trigger such a run-away reconnection/turbulence avalanche has to be satisfied. A quantitative description of such a critical condition is difficult, given the complicated physics involved in magnetic reconnection and turbulence. Nonetheless, one may envisage the following scenario (Fig.1):

- Initially, the field lines entrained in the ejecta are globally ordered. Since the poloidal field drops with radius more rapidly ($\propto R^{-2}$) than the toroidal

¹³ We note that the study of reconnection is an rapidly evolving field (Drake et al. 2006; Loureiro et al. 2007, 2009; Zenitani et al. 2009, 2010). Many questions still remain open.

field ($\propto R^{-1}$), the ordered field lines essentially lie in the plane of the ejecta front (i.e. perpendicular to the direction of motion of the ejecta). In the literature, two types of field configurations have been discussed for GRBs (e.g. Spruit et al. 2001): the “striped wind” geometry with alternating field configuration and the helical “jet-like” structure. The former is relevant for pulsar systems in which the magnetic axis is misaligned with the rotational axis. For GRB systems, unless the central object is a rapidly rotating millisecond magnetar, it is more likely that the magnetic axis is aligned with the rotational axis (e.g. in the black hole - torus systems). This leads to the helical magnetic field configuration. In the following, we will mostly focus on the helical structure, but will mention the striped wind geometry when relevant.

- Internal collisions in an unsteady outflow would alter the magnetic field configuration. Initially the field lines have a large coherent length ($\lambda_{\parallel} \sim R_{\theta}$). Since the most field lines have the same orientation, reconnection is very difficult to occur. Even if it occurs, since the condition to power a GRB (Eqs.[45] and [46]) is not satisfied, the reconnection process proceeds very slowly. Without significant magnetic dissipation, the collisions are essentially elastic. In any case, the ram pressure received by each magnetized shell during the collisions serves as the agent to distort the field lines. This is because in reality, all the fields (density, velocity and magnetic) are not uniform, and counter-streaming of the two fluids involved in a collision would amplify the perturbations to make the field lines more distorted. The scale of coherent length λ_{\parallel} would progressively reduce as collisions continue to occur. As a result, the parameter s would gradually decrease with radius (Fig.2).
- The first reconnection seed requires bringing together two sets of field lines with opposite orientations. This is easier to achieve for the striped wind geometry during the collision processes, but is more difficult for the helical geometry. In the majority of the locations for the helical configuration, the field lines in the two colliding shells have the same orientation. However, astrophysical systems are not perfectly symmetric systems. One may imagine some scenarios to trigger reconnection events at some locations. For example, current-driven kink instability may develop in the jet (e.g. Mizuno et al. 2009b), which would introduce a slight misalignment of the magnetic field axes in two consecutive “shells”. This would result in a small cross section near the magnetic axes that have opposite orientations in the two shells (Fig.3). The first seed reconnection would then occur.
- Once reconnection seed event is triggered, the rapid energy ejection from the reconnection layer would disturb the nearby ambient plasma and field lines to make the region more turbulent. The reconnection layer is also subject to various instabilities, e.g., the two-stream instability that develops as a consequence of reconnection accelera-

tion. The turbulence stirs the plasma to allow more opposite-orientation field lines approach each other, so that further reconnection events occur. These new reconnection events would eject more energy to make the ejecta more turbulent, leading to a reconnection-turbulence avalanche. This would result in a runaway catastrophic release of the stored magnetic field energy. Particles are accelerated either directly in the reconnection regions, or stochastically in the turbulent regions, which radiate synchrotron photons that power the observed GRB emission. The discharge process ceases when σ is reduced to $\sigma_{end} \leq 1 \ll \sigma_{ini}$. This is one ICMART event, which would compose one fundamental unit of a GRB (one pulse). Other collisions that trigger other reconnection-turbulence avalanches would give rise to other pulses in the GRB. A GRB event is the superposition of many individual ICMART events.

GRB events are relativistic in nature. Although the condition (45) or (46) gives the requirement for powering a GRB with global turbulent reconnection. In order to achieve such a relativistic reconnection/turbulence avalanche, some physical conditions may be needed.

The first relevant condition is the strength of the collisions that distort the field line configurations. We first comment on the role of internal shocks in these collisions. A common misconception is that shocks do not exist in the high- σ regime. This is not always true. It is relevant for the interaction between a strongly magnetized (high- σ) shell and a non-magnetized ($\sigma = 0$) medium (e.g. deceleration of a magnetized shell by the ISM). No shock can form in the high- σ shell if the thermal pressure in the shocked non-magnetized medium is smaller than the magnetic pressure in the magnetized shell (Zhang and Kobayashi 2005; Mizuno et al. 2009a)¹⁴. On the other hand, for the collision between two shells with the same σ value, even a moderate collision would give rise to an excess pressure (ram pressure) that exceeds the magnetic pressure. This would lead to a pair of shocks passing through both shells. For a given σ value, the strength of the shock increases with Γ_{fs} , and can reach more than 50% of the strength of a $\sigma = 0$ shock once Γ_{fs} exceeds 3 (Figs 1 & 2 of Zhang and Kobayashi 2005). So in the ICMART model essentially all the collisions are accompanied by internal shocks, but the main energy dissipation is not through internal shocks. What the shocks do is to disturb the velocity, density and magnetic fields. These distortions are reinforced via turbulence, which reduce λ_{\parallel} , until an ICMART event is eventually triggered. Without numerical simulations, it is hard to quantitatively analyze the role of internal shocks in the high- σ regime. Qualitatively, for the same σ value, a larger relative Lorentz factor between the two shells

¹⁴ The reverse shock forming condition introduced by Giannios et al. (2008) is erroneous. These authors claimed that there should be no reverse shock when $\sigma > 0.3$, but the later numerical simulations performed by the same group suggests that a weak reverse shock does exist in the $\sigma > 0.3$ regime (Mimica et al. 2009). The numerical result is consistent with Zhang and Kobayashi (2005) and Mizuno et al. (2009a) who suggested that the only physical condition to define the existence of a reverse shock in a magnetized ejecta is whether the forward shock pressure exceeds the magnetic pressure of the ejecta.

(Γ_{fs}) tends to introduce a larger perturbation in the ordered magnetic fields. Within the rest frame of shell 1, the ram pressure exerted by shell 2 is $P_{ram,21} = \Gamma_{21}^2 \rho_2' c^2$, which would be larger than its own magnetic pressure $P_{B,1} = B_1'^2 / 8\pi = (1/2)\rho_1' c^2 \sigma$, when

$$\Gamma_{21} \geq \left(\frac{1}{2} \sigma \frac{\rho_1'}{\rho_2'} \right)^{1/2} \quad (47)$$

is satisfied. This is the condition for a strong shock-induced-perturbation to occur.

A second relevant condition is that the outflow from a reconnection event has to be relativistic. This would induce relativistic turbulence, which is essential to induce turbulence-related GRB temporal variability (see more in Sect.5.1 below). The relativistic extension of Sweet-Parker and Petschek scenarios have been discussed by Blackman and Field (1994) and Lyutikov and Uzdensky (2003). Based on energy conservation conditions, these authors argued that under certain conditions, both the inflow and outflow speeds (V_{in} and V_{out}) can reach the relativistic regime. These treatments did not consider force balance across the reconnection layer, an effect becoming very important in the relativistic regime. Lyubarsky (2005) evaluated this effect and correctly concluded that V_{in} can never achieve the relativistic speed. In any case, in long term the condition imposed by energy conservation should be satisfied, so that the outflow can achieve a relativistic speed under certain conditions (Lyubarsky 2005, M. Lyutikov, 2010, private communication). This condition is essential to induce relativistic turbulence. The condition for a relativistic outflow may be approximated as $s < \sigma$ (e.g. Lyutikov and Uzdensky 2003), or, in terms of the Bohm diffusion limit

$$\lambda_{\parallel} < \sigma r'_{B,e} \simeq 9.3 \times 10^3 \text{ cm } \sigma_1 \gamma_{e,3} L_{w,52}^{-1/2} \Gamma_{2.5} R_{15} \left(\frac{1 + \sigma}{\sigma} \right)^{1/2} \quad (48)$$

This condition is more demanding than Eq.(46), which means that once relativistic turbulence is excited, the turbulent reconnection avalanche can naturally power a GRB.

3.6. Preference of a large emission radius

The ICMART events occur preferably at large radii from the central engine. This is because triggering an ICMART event requires that the conditions Eq.(45) and probably also Eq.(48) are satisfied, which demands λ_{\parallel} being small enough. Early collisions (typically at small radii) only serve to distort the field lines and do not directly trigger ICMART events. Statistically, shells that collide at large radii tend to have more distorted field configurations and hence, can more easily trigger ICMART events (Fig.1).

Observationally, it is not easy to infer the GRB emission radius R_{GRB} from the MeV data alone. However, by combining radiation information from other wavelengths, there are three independent, indirect ways to constrain R_{GRB} . (1) Swift observations suggest that the early X-ray afterglow light curves are dominated by a steep decay component (Tagliaferri et al. 2005), which is best interpreted as the high-latitude emission of the prompt GRB as the emission is abruptly ceased (Zhang et al. 2006). Within such an interpretation, the duration of the

tail defines the minimum of $R_{GRB}\theta_j$. The data suggest that R_{GRB} is typically large (say, $R_{GRB} \geq 10^{15}$ cm) if the high-latitude emission interpretation is valid (Lyutikov 2006a; Kumar et al. 2007). (2) Some GRBs have prompt optical detections or upper limits. If the optical emission arises from the same region as the MeV emission, then the brightness of the optical emission can be used to derive a constraint on R_{GRB} , based on the argument that synchrotron self-absorption should not suppress the optical flux. The bright optical prompt emission of GRB 080319B requires that the optical emission region has to be greater than 10^{16} cm (Racusin et al. 2008; Kumar and Panaitescu 2008), so that $R_{GRB} > 10^{16}$ cm is inferred if the MeV emission and optical emission originate from the same region (c.f. Fan et al. 2009; Zou et al. 2009). A systematic analysis of other prompt optical data (Shen and Zhang 2009) suggests that data are consistent with $R_{GRB} \geq 10^{14}$ cm. (3) If GeV emission is from the same region as the MeV component, as is inferred from most Fermi/LAT GRBs (Zhang et al. 2010), the detection of the high energy photons can be used to constrain both the emission radius and the bulk Lorentz factor (Gupta and Zhang 2008). Applying this method to GRB 080916C, the derived R_{GRB} is typically greater than 10^{15} cm (Zhang and Pe'er 2009). We can see that the three independent pieces of information generally point towards a consistent picture, namely, the GRB emission radius R_{GRB} is relatively large. This is consistent with the expectation of the ICMART model.

4. MERITS AND IMPLICATIONS OF THE ICMART MODEL

The ICMART model invokes internal collisions as the trigger of magnetic reconnection/turbulence avalanche. It therefore carries the merits of the internal shock model, namely, the emission site is ‘‘internal’’, and the central engine activity defines the main variability time scale (the pulses in the light curve)¹⁵. On the other hand, it can overcome or alleviate some of the drawbacks of the IS model as discussed in §2.1, which we elaborate in the following.

4.1. Radiative efficiency

Let's assume that two shells [(m_1, Γ_1) and (m_2, Γ_2)] with an initial σ_{ini} collide with each other, and that the collision triggers a reconnection/turbulence cascade that results in a catastrophic discharge of the magnetic energy. This leads to conversion of a significant amount of magnetic energy to internal energy of the fluid, and hence, to radiation. Let's envisage a picture where the two shells merge with a much lower magnetization parameter σ_{end} by the end of such an inelastic collision. Energy conservation

$$(\Gamma_2 m_2 + \Gamma_1 m_1)(1 + \sigma_{ini}) = \Gamma_m (m_1 + m_2 + U')(1 + \sigma_{end}) \quad (49)$$

and momentum conservation

$$(\Gamma_2 \beta_2 m_2 + \Gamma_1 \beta_1 m_1)(1 + \sigma_{ini}) = \Gamma_m \beta_m (m_1 + m_2 + U')(1 + \sigma_{end}) \quad (50)$$

give the same solution for Γ_m [Eq.(3)] as the IS model. The energy dissipation efficiency, on the other hand, is

¹⁵ Again this is also the merit of the dissipative photosphere model which does not demand internal collisions.

much larger, i.e.

$$\begin{aligned}\eta_{\text{ICMART}} &= \frac{\Gamma_m U'}{(\Gamma_1 m_1 c^2 + \Gamma_2 m_2 c^2)(1 + \sigma_{ini})} \\ &= \frac{1}{1 + \sigma_{end}} - \frac{\Gamma_m (m_1 + m_2)}{(\Gamma_1 m_1 + \Gamma_2 m_2)(1 + \sigma_{ini})} \\ &\simeq \frac{1}{1 + \sigma_{end}} \quad (\text{if } \sigma_{ini} \gg 1).\end{aligned}\quad (51)$$

This is $\sim 50\%$ if $\sigma_{end} \sim 1$, and can reach 90% if $\sigma_{end} \sim 0.1$. This can naturally account for the observed high radiative efficiency of most GRBs (Zhang et al. 2007).

4.2. Particle acceleration and the fast cooling problem

In an ICMART event, particles can be accelerated in the following two ways. First, particles are accelerated directly in the reconnection zone. This happens when particles are bounced back and forth between the oppositely directed approaching magnetic fluxes and gain energy during each gyration. It is similar to shock acceleration and is an efficient 1st order Fermi process (de Gouveia dal Pino and Lazarian 2005; Lazarian and Opher 2009). The second acceleration mechanism is the stochastic acceleration of particles in the turbulent region, which is a 2nd order Fermi process.

We defer the detailed discussion on particle acceleration and radiation spectrum of the ICMART model to a future work, but qualitatively discuss the difference between this model and the shock model. Within the standard internal shock model, particles are accelerated at the shock front via the 1st-order Fermi mechanism (Spitkovsky 2008; Baring and Summerlin 2009). After the shock passes through the shell, the downstream hot electrons would cool rapidly through synchrotron and inverse Compton emission. Once an electron is accelerated to a high energy, there is no further heating process, and the electron suffers radiative cooling. Such a scenario inevitably introduces the so-called fast cooling problem as discussed in §2.1.3, unless a much small-scale magnetic field is introduced (Pe’er and Zhang 2006; Asano and Terasawa 2009).

In the ICMART scenario, electrons do not undergo such a “one-shot” acceleration like in the shock scenario. Rather, they would be accelerated repetitively. This is because the ICMART avalanche happens globally in the dissipation region (unlike just near the shock front in the shock scenario). There is no distinct separation of the particle acceleration region and the cooling region. As a result, any particle would undergo multiple accelerations in the reconnection regions either directly or stochastic scattering of the constantly evolving turbulent field. For the 1st-order reconnection acceleration scenario, particle acceleration time could be much shorter than the cooling time scale, so that a power-law distributed electron population can be accelerated up to an energy at which cooling time scale balances the acceleration time scale (see Sect.4.3 below). This is similar to the shock scenario, in which the fast cooling problem remains. On the other hand, for the 2nd-order turbulence acceleration scenario the acceleration time can be long so that one may achieve a balance between cooling and heating. In the past, this was referred to as the “slow volume heating” scenario, which invokes Compton upscattering off emission from a dissipative photosphere (e.g. Thompson

1994; Ghisellini and Celotti 1999; Stern and Poutanen 2004; Pe’er et al. 2006; Giannios and Spruit 2007; Beloborodov 2010). The electron energy of these previous slow heating models is typically sub-relativistic, say, 10s-100s keV. In the ICMART scenario discussed here, the slow heating due to turbulent acceleration would happen in the relativistic regime if a significant fraction of the magnetic energy is transferred to particle energy via the 2nd order stochastic turbulence acceleration. This is due to the combination of two effects: a much reduced electron number in a high- σ flow (reduced by a factor $1 + \sigma$) and a much lower magnetic field at a much larger emission radius than photosphere (i.e. $R_{\text{ICMART}} \gg R_{ph}$). To show this, we assume that a fraction ξ of comoving magnetic energy is consumed through slow heating by turbulence acceleration. The average heating rate per electron in the emission region is $\dot{E}'_{heat} \simeq \xi U'_B \varepsilon_e / \Delta t' n'_e$, where ε_e is the fraction of the dissipated energy that is distributed to electrons. Noticing that the dominant cooling mechanism in a high- σ flow is synchrotron radiation, the average cooling rate can be estimated as $\dot{E}'_{cool} \simeq (4/3)\gamma_e^2 \sigma_T c U'_B$. Balancing heating and cooling to make $\dot{E}'_{heat} = \dot{E}'_{cool}$, one can solve for the critical electron energy below which slow heating dominates, i.e.

$$\begin{aligned}\gamma_{e,h} &= \left(\frac{3\xi\varepsilon_e}{4\sigma_T c \Delta t' n'_e} \right)^{1/2} \simeq 2.6 \times 10^3 \left(\frac{\xi\varepsilon_e}{Y} \right)^{1/2} \\ &\times L_{w,52}^{-1/2} \Gamma_{2.5}^{1/2} R_{15} m^{1/2} (1 + \sigma)_1^{1/2} \Delta t_{-3}^{-1/2},\end{aligned}\quad (52)$$

where $\Delta t' = \Gamma \Delta t$ has been used, and Δt has been normalized to 10^{-3} s, the minimum variability time scale detected in GRBs. Equation (52) therefore gives the maximum electron Lorentz factor below which slow heating dominates and fast cooling problem is no longer relevant. The corresponding synchrotron photon energy is then

$$\begin{aligned}E_h &\sim \hbar \Gamma \gamma_{e,h}^2 \frac{eB'}{m_e c} (1 + z)^{-1} \sim 23 \text{ keV} \left(\frac{\xi\varepsilon_e}{Y} \right) \\ &\times L_{w,52}^{-1/2} \Gamma_{2.5} R_{15} m (1 + \sigma)_1 \left(\frac{\sigma}{1 + \sigma} \right)^{1/2} \Delta t_{-3}^{-1} \left(\frac{1 + z}{2} \right)^{-1}\end{aligned}\quad (53)$$

In reality, both acceleration mechanisms would operate in the ICMART regions. The 1st-order reconnection acceleration likely dominates, which would define E_p and high energy emission of the GRB. If the 2nd-order turbulence acceleration can transfer a good fraction energy to particles so that ξ is not $\ll 1$, then E_h is close to E_p (Eq.[57] discussed in the next section). The fast cooling problem may be alleviated.

4.3. Electron number and E_p

The electron number excess problem of the internal shock model (§2.1.4) is naturally overcome in the ICMART model. This is because the baryon-associated electron number is simply $(1 + \sigma)^{-1}$ of that in the baryon-dominated model for the same L_w . In principle, pair production can increase the lepton number, but the large emission site related to the ICMART model is way above the pair photosphere (Mészáros et al. 2002; Kobayashi et al. 2002; Pe’er et al. 2006) so that pair production may not be effective. This makes the Lorentz factor of each electron increase by a factor of $(1 + \sigma)$ with respect to the baryon-dominated case, naturally raising E_p to the γ -ray band.

To quantitatively address this point, we investigate the typical energy of synchrotron radiation in a high- σ flow. Synchrotron radiation is the dominant mechanism in a Poynting-flux-dominated flow, since the photon energy density (relevant for inverse Compton scattering) is much smaller than the magnetic energy density. The spectral peak energy E_p in the ICMRT model can also be expressed as Eq.(5). The comoving magnetic field can be estimated according to Eq.(20). The factor $\sigma/(1+\sigma)$ ranges from ~ 1 (for $\sigma_{ini} \gg 1$ in the beginning of an ICMART event) to $\sim 1/2$ (for $\sigma_{end} \sim 1$ at the end of the ICMART event). Assuming that the particle acceleration is dominated by the 1st order reconnection acceleration, and that the energy release from magnetic dissipation is distributed to electrons and protons in the fractions of ε_e and ε_p with $\varepsilon_e + \varepsilon_p = 1$ (to be differentiated from ϵ_e , ϵ_p and ϵ_B in the shock case), one can write

$$\frac{L_w \eta}{4\pi R^2 c \Gamma^2} = n'_p \bar{\gamma}_p m_p c^2 + n'_e \bar{\gamma}_e m_e c^2 = n'_e \bar{\gamma}_e m_e c^2 / \varepsilon_e. \quad (54)$$

The comoving electron number density can be calculated by Eqs.(19) and (17). This gives

$$\bar{\gamma}_e = \eta \varepsilon_e (1 + \sigma) \frac{m_p + Y m_e}{Y m_e}. \quad (55)$$

The minimum electron Lorentz factor can be derived by $\gamma_{e,m} = \phi(p) \bar{\gamma}_e$. In the ICMART model, the observed gamma-ray luminosity can be expressed as

$$L_\gamma = L_w \eta \varepsilon_e. \quad (56)$$

one can then write E_p as

$$\begin{aligned} E_{p,ICMART} &\sim \frac{m_e c^2}{B_q} [\phi(p)]^2 \left(\frac{m_p + Y m_e}{Y m_e} \right)^2 \left(\frac{L_\gamma}{R_{ICMART}^2 c} \right)^{1/2} \\ &\times (1+z)^{-1} \left[\left(\frac{\sigma}{\eta \varepsilon_e (1+\sigma)} \right)^{1/2} (\eta \varepsilon_e)^2 (1+\sigma)^2 \right] \\ &\simeq 160 \text{ keV} \left(\frac{\phi(p)}{1/6} \right) L_{\gamma,52}^{1/2} R_{ICMART,15}^{-1} \\ &\times (\eta \varepsilon_e)^{3/2} \sigma_{1.5}^2 \left(\frac{1+z}{2} \right)^{-1}. \end{aligned} \quad (57)$$

Compared with the E_p expression in the IS model (Eq.[8]), the ICMART model can easily make E_p in the range of several hundreds of keV (as observed) by requiring $\sigma \sim$ several 10s.

By reducing the number of electrons, one can also naturally overcome the self-absorption problem introduced by the electron number excess problem (Shen and Zhang 2009).

4.4. Amati/Yonetoku relation

Comparing Eq.(8) and Eq.(57), we can see that E_p of the IS model and ICMART model both have the dependence $E_p \propto L_\gamma^{1/2}$. The problem of the IS model (as discussed in §2.1.5) is that R_{IS} has an additional dependence on Γ , which is correlated to L_γ (Liang et al. 2010). This completely destroys the $E_p \propto L_\gamma^{1/2}$ dependence. In the ICMART model, E_p has the dependence of $\propto L^{1/2} \sigma^2 R_{ICMART}^{-1}$. It is hard to analytically investigate how σ and R_{ICMART} influence the apparent $E_p \propto L_\gamma^{1/2}$ dependence. The sensitive dependence on σ suggests that a

small variation of σ would lead to a significant variation of E_p . On the other hand, the shallow dependence of σ on σ_0 (2/3 power) and R (-1/3 power) suggests that the variation of σ may not be significant. Also, an outflow with a higher σ would be more difficult to trigger an ICMART event, since it takes more stringent criteria (e.g. a larger Γ contract and more collisions) to distort the field lines (e.g. Eq.[47]). Therefore an ICMART event with a higher σ tends to happen at a larger R_{ICMART} . This would partially compensate the E_p scatter due to σ variation. If the $\sigma^2 R_{ICMART}^{-1}$ factor has a weak dependence on L_γ and does not have a large scatter, then one may obtain the Amati/Yonetoku correlation. Numerical simulations of various processes (e.g. magnetic field distortion during collisions, reconnection physics, and the trigger condition of ICMART events) are needed to verify or disprove such a speculation.

4.5. Weak photosphere

Within the ICMART picture, the σ value remains moderately high at R_{GRB} before strong magnetic field dissipation happens. This requires that the magnetic acceleration and dissipation effects are not prominent at the smaller radii. This guarantees a weak photosphere emission component (energy smaller by a factor of $(1+\sigma)^{-1}$ with respect to the baryon-dominated model), which satisfies the constraints of the GRB 080916C data (Zhang and Pe'er 2009).

5. PREDICTIONS OF THE ICMART MODEL

The ICMART model makes a list of predictions that may be used to differentiate it from other prompt emission models using the observational data.

5.1. Variability time scales: engine and turbulence components

The most important prediction of the ICMART model is that there are two mechanisms that define the observed GRB variability time scales. Since the emission is triggered by internal collisions, the internal wind irregularity inevitably leaves an imprint on the light curve. This engine-defined variability is similar to that of the internal shock model, and is relevant to a broader (“slow”) component of variability. The characteristic time scale of this component is defined by the angular spreading time at the large emission radius, which reads $R_{ICMART}/\Gamma^2 c \sim 0.3 \text{ s } R_{ICMART,15} \Gamma_{2.5}^{-2}$. Phenomenologically, this corresponds to individual broad “pulses” of the light curves, which is visible in some GRBs. On the other hand, within each ICMART emission region (the broad pulse), there are many turbulent regions from which highly variable emission is released. This corresponds to a second variability component with very small time scales. In the previous GRB models, the variability time in all scales are either defined by the central engine (Sari and Piran 1997) or by relativistic turbulence (Narayan and Kumar 2009). The ICMART model suggests that the observed GRB variability is the superposition of these two components. The two variability components may be differentiated via a proper temporal analysis of GRB light curves.

Visually some GRB light curves do show several visible slow bumps superposed by rapid variability features

(Fig.4). Power density spectrum analyses using Fourier transform (Beloborodov et al. 2000), however, did not reveal distinct two-component variability distributions. Nonetheless, studies using some more sophisticated statistical methods have started to reveal the evidence for two variability components at least for some GRBs (e.g. Shen & Song 2003; Vetere et al. 2006, see also H. Gao et al. 2010, in preparation; R. Margutti et al. 2010, in preparation).

5.2. E_p evolution within a pulse

In the ICMART model, one ICMART event (triggered by one collision) corresponds to one pulse in the GRB light curve. During each event, since the magnetic energy is continuously converted to the particle energy and then released as radiation, one may approximately treat the plasma as having σ continuously decrease with time while the lepton number not changed. According to Eq.[57], the peak energy in the ICMART model evolves as $E_p \propto L_\gamma^{1/2} \sigma^2$. Although L_γ increases shallowly during the rising phase, the steep dependence on σ compensates this. Noticing that during the rising phase L_γ only increases by a factor of a few while σ drops 1-2 orders of magnitudes, one expects that in general E_p decreases throughout a pulse (the fundamental radiation unit) in GRB prompt emission (Fig.4), probably with a steepening in decay after the light curve peak. Observationally, the majority of GRB pulses indeed show a hard-to-soft evolution behavior (Norris et al. 1986; Ford et al. 1995; Lu et al. 2010), which is consistent with the expectation of the ICMART model. On the other hand, a small fraction of pulses show the so-called “tracking” behavior, i.e. the hardness of the spectrum is positively correlated with the flux variation across the pulse (Golenetskii et al. 1983). These pulses cannot be related to an ICMART event. It may, however, be interpreted by emission from a turbulent eddy, with the rising and decaying components corresponding to entry and exit of the eddy from the field of view (Γ^{-1} cone). This requires the existence of a large scale eddy that can give rise to a broad pulse in the GRB light curve.

5.3. Gamma-ray polarization evolution within a pulse

Since the ICMART process destroys the ordered global magnetic fields in the ejecta, one naturally expects an evolution of the linear polarization degree in the γ -ray emission during each ICMART unit, i.e. a pulse. The initial gamma-ray polarization degree may be close to the maximum value achievable for synchrotron emission in an ordered magnetic field, i.e. $\Pi \sim 50\% - 60\%$ (Lyutikov et al. 2003; Granot 2003). At the end of the ICMART event, the ordered field structure would be largely destroyed. However, even in the fully turbulent limit, the net polarization degree would not become zero, since in the strong field regime, turbulence is anisotropic with eddies elongated along the local field lines. The average polarization in the Γ^{-1} -cone field of view would not be zero. Without detailed numerical simulations of an ICMART event (which requires a dissipative, relativistic MHD with the details of reconnection processes delineated, and which is beyond the scope of all the current GRB motivated MHD simulations), it is hard to quantitatively predict the polarization degree at the end

of the ICMART event. Nonetheless, a value of $\Pi \sim$ a few% – 10% may be reasonable. Since different pulses correspond to different ICMART events in our model, we expect a significant polarization degree evolution during the GRB prompt phase, with Π starting with a high value at the beginning of each pulse and evolving from high to low across the pulse (Fig.4). For bursts with overlapping pulses, the Π evolution would be more complicated since it reflects the superposition of the contributions of different pulses.

Observationally, there is no robust gamma-ray polarization detection yet. Coburn and Boggs (2003) reported $\Pi = 80\% \pm 20\%$ for GRB 021206 using the RHESSI data. However the conclusion cannot be confirmed by an independent analysis of the same data (Rutledge and Fox 2004; Wigger et al. 2004). Willis et al. (2005) derived lower limits of the polarization degree $\Pi > 35\%$ and $\Pi > 50\%$ for GRB 930131 and GRB 960924, respectively, using the BATSE Albedo Polarimetry System (BAPS), but could not strongly constrain the degree of polarization beyond a systematics-based estimation. Another polarization measurement for the INTEGRAL burst GRB 041219A (Kalemci et al. 2007; McGlynn et al. 2007) is also subject to large uncertainty. Nonetheless, these studies show the tentative evidence that GRB γ -ray emission may be polarized. A true breakthrough could be made by one of several proposed γ -ray polarimeters that are suitable to detect polarized γ -rays from transient sources, e.g. POET (Hill et al. 2008), POLAR (Lamanna et al. 2008), and PoGO (Mizuno et al. 2005). For example, for completely ordered magnetic fields, POET can measure the polarizations of $> 30\%$ of bursts detected by the mission (Toma et al. 2009b). The unique time-dependent Π evolution pattern predicted for the ICMART model may be tested by future observations with these detectors.

5.4. Polarized external reverse shock emission

Regardless of the composition of the GRB ejecta, the outflow is eventually decelerated by a circumburst medium, be it a constant density interstellar medium (ISM), or a stratified stellar wind (Mészáros and Rees 1997a; Sari et al. 1998; Dai and Lu 1998; Chevalier and Li 2000). Before entering the self-similar deceleration regime (Blandford and McKee 1976), a reverse shock may propagate into the ejecta to decelerate it. The composition of the ejecta does affect the radiation signature from the reverse shock (Zhang and Kobayashi 2005). In particular, the reverse shock emission is expected not to be bright or is completely suppressed if σ is very small (Fan et al. 2004b; Nakar and Piran 2004; Jin and Fan 2007) or very large (Zhang and Kobayashi 2005; Mimica et al. 2009). A bright optical flash may be detected if $\sigma \lesssim 1$, as is discovered in some GRBs such as GRB 990123 (Fan et al. 2002; Zhang et al. 2003; Kumar and Panaitescu 2003; Gomboc et al. 2008). At a slightly higher $\sigma \geq 1$, the reverse shock emission brightness drops significantly.

In the ICMART model, the final σ value after the magnetic dissipation would be close to (maybe slightly below) unity, based on an energy equipartition argument. The exact σ value is hard to predict and is subject to many uncertainties. In any case, similar to the discussion of prompt γ -ray polarization above, the reverse shock op-

tical emission should also be somewhat polarized (say, a few percent). If polarimetric observations can be carried out during the early rapidly decaying phase due to the reverse shock emission (say, in the optical band), a polarized optical signal should be detected. Observations of early optical polarimetry are now regularly carried out by some groups, e.g. the Liverpool optical polarization observation group. Measurements of early optical polarimetry have been made for two GRBs. For GRB 060418, which shows a smooth deceleration bump that is likely due to the forward shock emission, an upper limit of $\Pi < 8\%$ was set up (Mundell et al. 2007). Since the forward shock is the emission of shocked circumburst medium, this low level polarization is entirely consistent with the theoretical expectation. On the other hand, recently the team detected a $\Pi = 10\% \pm 2\%$ optical polarization from GRB 090102 (Steele et al. 2009). The polarized signal was measured during the rapid decay phase of the early optical light curve, which is consistent with being the reverse shock emission with $\sigma < 1$. This observational fact is consistent with the expectation of the ICMART model. More future early optical polarimetric data are needed to further test this prediction of the ICMART model.

5.5. No detectable synchrotron self-Compton spectral component during GRB prompt emission

According to the ICMART model, throughout the GRB prompt emission phase, one has $\sigma \geq 1$ in the emission region. The Compton parameter \mathcal{Y} is therefore $\ll 1$. The magnetic field energy density is much larger than the synchrotron photon energy density, so the SSC process is greatly suppressed. One therefore expects no extra high energy emission features other than extrapolation of the MeV spectrum (Band spectrum) to high energy. This is consistent with the observations of the majority of Fermi LAT GRBs, including GRB 080916C (Zhang et al. 2010).

6. GRB 080916C

In this section we discuss GRB 080916C within the ICMART model. This is the first bright Fermi/LAT burst whose time-dependent broad band spectra are measured. The observational results are somewhat surprising for theorists. Three theoretically motivated features, namely the pair cutoff feature at high energy, the SSC component at high energy, and the quasi-blackbody photosphere emission component are all missing. Instead, the time dependent spectra are a set of nearly featureless “Band” functions ranging from ~ 10 keV to ~ 10 GeV (Abdo et al. 2009; Zhang et al. 2010). In order to interpret this burst within the baryonic models, one needs to introduce several spectral components that conspire to mimic a Band function covering 6-7 orders of magnitude. For example, the model developed by Toma et al. (2009) invokes SSC in the internal shock, upscattered cocoon emission, as well as another synchrotron emission component to model the observed Band function spectrum. The neutron-heating photosphere model developed by Beloborodov (2010) needs to attribute the very high energy emission to a different component (e.g. from the external shock, Kumar and Barniol Duran 2009; Ghisellini et al. 2010). The low energy slope below E_p is predicted to be $\alpha = 0.4$,

much harder than the observed $\alpha \sim -1$ slope in most of the epochs (Abdo et al. 2009). Another model developed by Li (2010a) applies the standard internal shock synchrotron emission to account for the emission near E_p , while invokes a series of residual internal shocks from which the IC emission spectra are superposed to account for the emission above 100 MeV. Finally, Razzaque et al. (2010) invokes a standard leptonic synchrotron component to interpret the MeV emission, while introduces a hadronic proton synchrotron emission component to account for emission above 100 MeV. All these models require fine tuning of their model parameters to account for a very simple broad-band Band spectrum that covers 6-7 orders of magnitude in all the time intervals, as is revealed by detailed time-dependent spectral analyses (Abdo et al. 2009; Zhang et al. 2010). Furthermore, none of these models have calculated the contribution of the photosphere emission (except Beloborodov 2010, who discussed the photosphere model itself), but rather raised some simple arguments (without calculation) to avoid the missing bright photosphere problem raised by Zhang and Pe’er (2009). A careful calculation by Fan (2010) showed that the Zhang-Pe’er argument cannot be circumvented even under the most favorable condition to “hide” the photosphere component.

The featureless Band function can be straightforwardly interpreted within the ICMART model. The lack of the three theoretically expected features is understandable within the ICMART model. 1. Since the emission radius is large for ICMART events (§3.6), the pair production opacity is reduced, so that the rest-frame ~ 70.6 GeV photon can escape the emission region. One therefore does not expect a pair cutoff feature in the spectrum. 2. Since the outflow is magnetically dominated in the comoving frame (i.e. $\sigma > 1$), the magnetic energy density is naturally much larger than the synchrotron photon energy density. The Compton parameter \mathcal{Y} is $\ll 1$. One therefore does not expect a SSC component in the high energy regime. 3. The “hot” component only carries a luminosity which is $(1 + \sigma)^{-1}$ times L_w . As a result, the photosphere emission is much dimmer, which can be hidden beneath the non-thermal emission component from the ICMART event (Zhang and Pe’er 2009).

Within the ICMART model, the entire Band function spectrum is one emission component, which is powered by synchrotron emission of the electrons accelerated in the ICMART events. GRB 080916C has an observed E_p ranging from 400 – 1200 keV in various time intervals (Abdo et al. 2009). At $z \sim 4.35$, its average luminosity in the first two main pulses is of the order of $\sim (1 - 2) \times 10^{53}$ erg s $^{-1}$. From Eq.(57), one could estimate the required σ for this burst

$$\sigma \sim (38 - 67)(\eta\varepsilon_e)^{-3/4} R_{\text{ICMART},15}^{1/2}. \quad (58)$$

Since $(\eta\varepsilon) \leq 1$, the estimate Eq.(58) is fully consistent with the independent constraint $\sigma > (15 - 20)$ based on the non-detection of the photosphere component (Zhang and Pe’er 2009). One can also estimate the maximum synchrotron emission energy in the ICMART model. Similar to the shock model, the maximum electron Lorentz factor is defined by equating the comoving acceleration time scale $t'_{acc} = \kappa\gamma_e m_e c / eB'$ (where $\kappa \geq 1$ is a parameter to denote the efficiency of particle acceleration) and the electron cooling time scale

$t'_c = 3m_e c / 4\gamma_e \sigma_T U'_B$ (where σ_T is the Thomson scattering cross section, and $U'_B = B'^2 / 8\pi$ is the comoving magnetic field energy density). This gives

$$\gamma_{e,M} = \left(\frac{6\pi e}{\sigma_T \kappa B'} \right)^{1/2} \simeq 1.2 \times 10^8 \kappa^{-1/2} B'^{-1/2}. \quad (59)$$

Noticing that the synchrotron spectral function $F(x)$ has a maximum value at $x = 0.286$ (Rybicki and Lightman 1979), the maximum electron synchrotron emission energy is

$$\begin{aligned} E_M &= 0.286 \frac{3}{4\pi} \hbar \Gamma \gamma_{e,M}^2 \frac{eB'}{m_e c} (1+z)^{-1} \\ &\simeq 13 \text{ GeV } \Gamma_3 \kappa^{-1} \left(\frac{1+z}{5.35} \right)^{-1}. \end{aligned} \quad (60)$$

The expression is similar to the shock acceleration case (e.g. Wang et al. 2009), although κ can vary depending on the instability growth rate in the ICMART cascade. In any case, the observed maximum photon energy 13.2 GeV can be interpreted given a large enough $\Gamma_3 > 1$ and a not too large κ . A large Γ is consistent with the constraint derived from the opacity argument (Zhang and Pe'er 2009). Alternatively, photons above 100 MeV may be originated from the external shock (Kumar and Barniol Duran 2009; Ghisellini et al. 2010)¹⁶. The requirement for κ and Γ is then much less demanding.

Another interesting feature of GRB 080916C is the delayed onset of the LAT band emission. In fact, most of the multi-component models discussed in the literature (Toma et al. 2009; Li 2010a; Razzaque et al. 2010) are motivated to interpret this feature. To us, this feature may be straightforwardly interpreted in the following way. The particle acceleration details could be different during the first ICMART event than the later ones. Either the electron spectral index is steeper, or there is a pair cutoff feature in the LAT band (the latter may be related to a smaller Γ or a smaller emission radius).

7. CONCLUSIONS AND DISCUSSION

We have developed a GRB prompt emission model in the high- σ regime, namely, the Internal-Collision-induced Magnetic Reconnection and Turbulence (ICMART) model. This model is motivated by the Fermi observations of GRB 080916C (Abdo et al. 2009), and developed upon the idea that GRBs are powered by 3D turbulence reconnection discussed by Lazarian et al. (2003) (but in the high- σ regime). This model inherits the merits of the internal shock and other models, but may overcome several drawbacks of the internal shock model (low efficiency, fast cooling, electron number excess, Amati/Yonetoku relation inconsistency, missing bright photosphere component, etc). The basic ingredients of the model include the following.

- The outflow launched from the GRB central engine has a high magnetization, i.e. $\sigma \gg 1$. The σ value

does not decrease significantly before reaching the GRB emission radius R_{GRB} , so that at R_{GRB} , one still has $1 \lesssim \sigma \lesssim 100$. As a result, the photosphere emission is not bright, and the observed emission is dominated by the non-thermal emission released during the ICMART events.

- The central engine is intermittent, launching an unsteady wind with variable luminosity and Lorentz factor. The wind interacts internally via collisions.
- Most collisions at small radii from the central engine do not result in significant energy dissipation. They mainly serve to distort the field lines, making the field configuration progressively irregular.
- At a certain large radius, the condition for turbulent magnetic field reconnection is satisfied. Reconnection events rapidly eject energetic particles to the ambient, which further drive turbulence. This results in a run-away discharge of the magnetic field energy in a reconnection/turbulence avalanche. This is one ICMART event, which corresponds to one broad GRB pulse. During the magnetic field energy discharge, the σ value drops from the original value to around unity.
- A GRB is composed of several ICMART events (i.e. broad pulses), each marks a catastrophic event to destroy ordered magnetic field lines. The peak energy E_p is expected to drop from high to low across each pulse. The γ -ray polarization degree is also expected to drop from $\sim 50 - 60\%$ to \sim a few % during each pulse. The magnetic field configuration at the end of prompt emission is largely randomized, but still has an ordered component. The reverse shock emission is expected to be moderately polarized.
- The GRB light curves should have two variability components, a broad (slow) component related to the central engine activity, and a narrow (fast) component associated with the relativistic magnetic turbulence.

This model differs from other magnetic GRB prompt emission models proposed in the past. The EM model proposed by Lyutikov and Blandford (2003) invokes an extremely high- σ ($\sigma > 10^6$) at the deceleration radius, which might not be realized in nature. The variability in this model has no direct connection with the central engine activity, while the evidence of an engine-related variability (e.g. those in X-ray flares) is mounting. A large number of GRB magnetic models are in the MHD regime (Thompson 1994; Spruit et al. 2001; Drenkhahn and Spruit 2002; Vlahakis and Königl 2003; Giannios 2008; Komissarov et al. 2009). These models invoke magnetic dissipation at smaller radii to enhance the photosphere emission. At large radii, it is assumed that the outflow is no longer Poynting-flux-dominated, so that the internal shock model can still operate. On the other hand, in the ICMART model it is envisaged that rapid reconnection/turbulence cascade only happens under a certain trigger condition, preferably at a large emission radius when the field lines are sufficiently distorted. So the main difference between the ICMART model and

¹⁶ This requires a high degree of coincidence since a detailed time-dependent spectral analysis with as many time bins as possible still reveals a series of nearly featureless Band-function spectra for all the time bins (Zhang et al. 2010). In any case, all the arguments for the ICMART model discussed in this paper are not affected even if > 100 MeV photons are of the external shock origin.

other MHD models is whether the magnetic energy is released abruptly at a large radius or continuously at small radii.

The physics invoked in this model is complicated. In this paper, we only limit ourselves to an analytical, qualitative delineation of the general picture of the model. Many ingredients of the model, such as magnetic acceleration in a high- σ flow, collision physics of high- σ shells (shocks and magnetic field distortion), reconnection physics, particle acceleration (1st-order vs. 2nd-order Fermi acceleration) and radiation, are introduced based on the best known results from the literature. Many speculations are subject to quantitative analyses and numerical simulations to verify. Further investigations are needed and indeed in plan.

Within the ICMART model, since the baryon number is smaller by a factor of $(1 + \sigma)^{-1}$ than the pure baryonic model, the expected hadronic radiation is also smaller by the same factor. Internal shocks have been proposed as the source of ultrahigh energy cosmic rays (UHECRs, Waxman 1995) and PeV neutrinos (Waxman and Bahcall 1997). The ICMART processes can in principle also accelerate protons to ultrahigh energies. However, the UHECR flux from a high- σ GRB is smaller by a factor of $(1 + \sigma)^{-1}$ than a baryon-dominated GRB. If the majority of GRBs have high- σ , then GRBs cannot be the dominant contributor to the observed UHECRs in the solar neighborhood. Similarly, the predicted diffuse PeV neutrino background is also lowered by a factor of $(1 + \sigma)^{-1}$. This makes it more challenging for km^3 neutrino telescopes (e.g. Icecube) to detect these neutrinos from GRBs¹⁷.

On the other hand, the GRB composition may be diverse, namely, the σ value may vary in a wide range among GRBs. For example, another LAT burst GRB 090902B shows a clear time-evolving blackbody component superposed on a non-thermal power law component (Ryde et al. 2010; Zhang et al. 2010), which is almost certainly the baryonic photosphere component. This burst is likely originated from a baryonic fireball proposed by Paczyński (1986) and Goodman (1986), see Pe'er et al (2010) for a more detailed discussion. However, GRB 090902B is a special event. Its special spectral feature is unique within the Fermi LAT GRB sample of Zhang et al. (2010). Most LAT GRBs have

¹⁷ Our discussion is relevant to traditional high luminosity GRBs. The nearby low-luminosity GRBs may be more abundant (Liang et al. 2007; Virgili et al. 2009). So far there is no strong evidence that they are Poynting flux dominated. If they

clear Band-only time-resolved spectra similar to GRB 080916C, which are good candidates for the ICMART scenario (Zhang et al. 2010). The ICMART model proposed here therefore can be applied to most GRBs.

The ICMART scenario developed in this paper may be also applied to other astrophysical objects, such as active galactic nuclei (AGNs). For example, two blazars (Mrk 501 and PKS 2155-304) were detected to have a 3-5 minute TeV variability (Albert et al. 2007; Aharonian et al. 2007), much shorter than the inferred light-crossing times at the black hole horizon. The detections of the TeV photons also require a Lorentz factor much larger than that inferred from the large scale jet modeling. The data demand some small-scale enhanced emission units (Begelman et al. 2008; Giannios et al. 2009). Suppose that an intermittent, moderately high- σ outflow is launched by the supermassive black hole central engine from these blazars, ICMART events similar to what are discussed in this paper may occur, which would produce small-scale turbulent emission units whose size is much smaller than the black hole event horizon. These turbulent eddies are relativistic, and hence, would give an extra Lorentz boost to the comoving emission. This would account for the observed rapid TeV variability and the apparent large Lorentz factor of the TeV emission regions of these two blazars.

This work is supported by NASA NNX09AT66G, NNX10AD48G, NNX10AP53G, and NSF AST-0908362 (BZ) and by a 985 grant at Peking University and Arizona Prize Fellowship (HY). We thank the anonymous referee for constructive comments. We also acknowledge helpful communications with or comments from the following colleagues on various topics discussed in this paper: J. Arons, A. M. Beloborodov, R. D. Blandford, Z.-G. Dai, F. Daigne, E. M. de Gouveia Dal Pino, Y.-Z. Fan, Z. Li, E.-W. Liang, S. Kobayashi, S. S. Komissarov, A. Königl, P. Kumar, A. Lazarian, D. Lazzati, M. Lyutikov, J. C. McKinney, M. V. Medvedev, P. Mészáros, Y. Mizuno, S. Nagataki, E. Nakar, R. Narayan, K.-I. Nishikawa, R. Ouyed, A. Pe'er, T. Piran, D. Proga, J. Poutanen, S. Razzaque, A. Spitkovsky, K. Toma, X.-Y. Wang, X.-F. Wu, and B.-B. Zhang.

are matter-dominated, they can be important contributors to diffuse high energy neutrinos and UHECRs (Gupta and Zhang 2007; Murase et al. 2006, 2008).

APPENDIX NOTATION LIST

The notation we used is listed in Table 1.

c	speed of light
c_s	speed of sound
d	separation between shells in the lab frame, $= c\delta t$
d_{\max}, d_{\min}	maximum and minimum separation between shells
e	electron charge
h	Planck constant
\hbar	reduced Planck constant
k	Boltzmann constant or turbulence wave number
k_{\perp}, k_{\parallel}	MHD turbulence wave number in the direction perpendicular/parallel to the magnetic field
l, l'	mean free path of microscopic interactions in the lab frame and comoving frame, respectively
$l'_{e,col}$	comoving mean free path of electron Coulomb collision
m	a dimensionless parameter defined as $1 + Ym_e/m_p$
m_1, m_2	mass of shell 1 and shell 2
m_e, m_p	electron rest mass, proton rest mass
n	particle number density of the GRB outflow in the lab frame
n_e, n'_e	electron number density in the lab frame and comoving frame
n_p, n'_p	proton number density in the lab frame and comoving frame
n_{GJ}	Goldreich-Julian charge number density of the GRB outflow in the lab frame
p	power law spectral index of particles (electrons or protons)
$r'_{B,e}, r'_{B,p}$	comoving electron gyro-radius and proton gyro-radius
r_{col}	strong Coulomb collision radius
s	dimensionless parameter defined in Eq.(43)
t'_{acc}	comoving particle acceleration time scale
t'_c	comoving cooling time scale
t'_{dyn}	comoving dynamical time scale
v'_e	comoving electron speed
z	redshift
B, B'	magnetic field strength in the lab frame and comoving frame
\mathbf{B}	magnetic field vector in the lab frame
B_q	critical magnetic field strength
E	observed photon energy
E_h	the critical photon energy below which slow heating effect is important
E_M	maximum observed photon energy
\mathbf{E}	electric field vector in the lab frame
E_p	observed spectral peak energy of GRB
$E_{\gamma,iso}$	isotropic gamma-ray energy of GRB
$E(k)$	turbulence energy per unit wave number at the wave number k
$E(k_{\perp}), E(k_{\parallel})$	turbulence energy per unit wave number at the wave number k_{\perp} , and k_{\parallel}
$E(\theta)$	GRB effective “isotropic” energy at an angle θ from the jet axis
$\dot{E}'_{heat}, \dot{E}'_{cool}$	comoving average heating and cooling rate of electrons
$F(x)$	a function to denote synchrotron emission spectrum of a single particle
F_b	matter flux: sum of baryonic and leptonic fluxes. Usually baryonic flux dominated.
F_P	Poynting flux
\mathbf{J}	current density vector
L	characteristic length scale of the flow
\mathcal{L}	length of reconnection layer
L_w	the total (including kinetic and magnetic) isotropic luminosity of the GRB ejecta (wind)
L_{γ}	the isotropic γ -ray luminosity of the GRB
$N(E)$	number of photons in the energy bin $(E, E + dE)$
$N(\gamma_e)$	number of electrons in the Lorentz factor bin $(\gamma_e, \gamma_e + d\gamma_e)$
P	pressure
P_{gas}	gas pressure
P_{mag}	magnetic field pressure
$P_{ram,21}$	ram pressure exerted to shell 1 by shell 2
R	radius from the central engine
R_{dec}	GRB ejecta deceleration radius
R_e	Reynold's number
R_{GRB}	radius of GRB prompt emission from the central engine
R_{ICMART}	radius of the ICMART events
R_{IS}	internal shock radius defined in Eq.(2)
R_m	magnetic Reynold's number
R_{MHD}	radius from central engine where the MHD condition is broken
R_{θ}	jet cross section radius at the radius R
S	Lundquist number
T	characteristic temperature of plasma
T_e, T_p	characteristic electron temperature, proton temperature
$T_{e,c}$	critical electron temperature for collisional/collisionless regime separation
U'	total internal energy in the internal shock or ICMART event
U'_B	comoving magnetic field energy density
U'_{ph}	comoving photon energy density
\mathbf{V}	velocity vector of the GRB fluid
V_{in}	incoming speed of the magnetic field lines in Sweet-Parker reconnection
V_{out}	the eventual outgoing speed in a reconnection event
V_A	Alfvén speed in general
V'_A	comoving Alfvén speed
$V_{A,NR}$	comoving Alfvén speed in the non-relativistic regime
$V'_{rec,loc}, V'_{rec,global}$	comoving local and global reconnection speed
x	argument of function $F(x)$

Y	number of leptons associated with each proton
\mathcal{Y}	The Compton parameter
α	GRB photon spectral index below E_p
β	dimensionless speed V/c or ratio between gas pressure and magnetic field pressure
β_f	dimensionless speed of the fast shell
β_m	dimensionless speed of the merged shell
β_s	dimensionless speed of the slow shell
γ_A	Alfvén Lorentz factor in general
γ'_A	comoving Alfvén Lorentz factor
γ_e	comoving electron Lorentz factor
$\gamma_{e,c}$	comoving electron Lorentz factor at cooling break
$\bar{\gamma}_e$	comoving mean electron Lorentz factor
γ_m, γ_M	minimum and maximum Lorentz factor of a power-law distributed proton or electron population
$\gamma_{e,m}$	minimum comoving electron Lorentz factor in an injected power law energy spectrum
$\gamma_{e,M}$	maximum comoving electron Lorentz factor in an injected power law energy spectrum
$\gamma_{e,p}$	comoving electron Lorentz factor that contributes to E_p in the synchrotron radiation model
γ_p	comoving proton Lorentz factor
$\bar{\gamma}_p$	comoving mean proton Lorentz factor
γ_{in}	Lorentz factor of incoming magnetic field lines for relativistic reconnection
Γ	GRB ejecta bulk Lorentz factor
Γ_0	the ejecta bulk Lorentz factor at the central engine
Γ_1, Γ_2	Lorentz factor of shell 1 and shell 2
Γ_{21}	relative Lorentz factor between shell 2 and shell 1
Γ_{43}	relative Lorentz factor between regions 4 (unshocked trailing shell) and 3 (shocked trailing shell)
Γ_f	Lorentz factor of the fast shell
Γ_m	Lorentz factor of the merged shell
Γ_s	Lorentz factor of the slow shell
Γ_{fs}	relative Lorentz factor between the fast and slow shells
Γ_{ud}	relative Lorentz factor between upstream and downstream
Γ_{max}	maximum Lorentz factor in the GRB ejecta
Γ_{min}	minimum Lorentz factor in the GRB ejecta
Γ_{tot}	achievable Lorentz factor of high- σ shell for total conversion of Poynting energy to kinetic energy
δ	thickness of reconnection layer
δ'_e, δ'_p	comoving electron and proton plasma skin depth
δt	duration between the end of ejecting a leading shell and the beginning of ejecting a trailing shell
δt_{max}	maximum δt in the ejecta
δt_{min}	minimum δt in the ejecta
δV	relative velocity of the flow
Δ	shell width in the lab frame
Δ'	shell width in the comoving frame
Δ_f	width of the fast shell
Δ_s	width of the slow shell
Δ_{max}	maximum shell width in the GRB ejecta, $= c\Delta t_{max}$
Δ_{min}	minimum shell width in the GRB ejecta, $= c\Delta t_{min}$
Δt	duration of central engine activity for each mini-shell in the ejecta
$\Delta t'$	comoving time scale for global magnetic dissipation within a shell with comoving width Δ'
Δt_{max}	maximum Δt in the ejecta
Δt_{min}	minimum Δt in the ejecta
ϵ_B	fraction of internal energy that is distributed to magnetic fields in internal shocks
ϵ_e, ϵ_p	fraction of internal energy that is distributed to electrons and protons in internal shocks
$\varepsilon_e, \varepsilon_p$	fraction of dissipated magnetic energy distributed to electrons and protons in an ICMART event
η	magnetic diffusion coefficient or energy dissipation efficiency in general
η_{IS}	energy dissipation efficiency of an internal shock
η_{ICMART}	energy dissipation efficiency of an ICMART event
θ	angle from the GRB jet axis
θ_j	GRB jet opening angle
κ	a parameter to denote efficiency of particle acceleration
λ_B	coherence length of a random magnetic field
$\lambda_{ }$	local reconnection length
ν	kinematic viscosity
ξ	fraction of comoving magnetic field energy that is dissipated through slow heating mechanism
Π	linear polarization degree
ρ	mass density in the lab frame
ρ'	mass density in the comoving frame
ρ'_1, ρ'_2	comoving mass density of the shell 1 and shell 2
σ	magnetization parameter as defined in Eq.(1)
σ_0	initial σ value at the GRB central engine
σ_c	critical σ value to separate the sub-Alfvén regime from the super-Alfvén regime
σ_{end}	final σ value after an ICMART event
σ_{ini}	initial σ value before an ICMART event
σ_T	Thomson scattering cross section
τ'_{col}	comoving Coulomb collision time
$\tau'_{col,NR}$	non-relativistic comoving Coulomb collision time
$\tau'_{col,R}$	relativistic comoving Coulomb collision time
τ_ν	viscous diffusion time
τ_{dif}	magnetic resistive diffusion time
τ_f	flow time scale
$\phi(p)$	a function of p to connect minimum particle energy with the mean energy
$\omega'_{B,e}, \omega'_{B,p}$	comoving electron and proton gyro-frequency
$\omega_{p,e}, \omega_{p,p}$	comoving electron and proton plasma frequency

REFERENCES

- Abdo, A. A., et al. 2009, *Science*, 323, 1688.
- Aharonian, F., et al. 2007, *ApJ*, 664, L71.
- Albert, J., et al. 2007, *ApJ*, 669, 862.
- Amati, L., et al. 2002, *A&A*, 390, 81.
- Asano, K., & Terasawa, T. 2009, *ApJ*, 705, 1714.
- Band, D., et al. 1993, *ApJ*, 413, 281.
- Band, D. L., & Preece, R. D. 2005, *ApJ*, 627, 319.
- Baring, M. G., & Sumnerlin, E. J. 2009. In X. Ao & G. Z. R. Burrows (Ed.), *American Institute of Physics Conference Series*, Volume 1183 of *American Institute of Physics Conference Series*, pp. 74–84.
- Barthelmy, S. D., et al. 2005, *ApJ*, 635, L133.
- Begelman, M. C., Fabian, A. C., & Rees, M. J. 2008, *MNRAS*, 384, L19.
- Begelman, M. C., & Li, Z.-Y. 1994, *ApJ*, 426, 269.
- Beloborodov, A. M. 2000, *ApJ*, 539, L25.
- Beloborodov, A. M. 2010, *MNRAS*, 407, 1033
- Beloborodov, A. M., Stern, B. E., & Svensson, R. 2000, *ApJ*, 535, 158.
- Beskin, V. S., Kuznetsova, I. V., Rafikov, R. R. 1998, *MNRAS*, 299, 341
- Blackman, E. G., & Field, G. B. 1994, *Physical Review Letters*, 72, 494.
- Blandford, R. D., & McKee, C. F. 1976, *Physics of Fluids*, 19, 1130.
- Burrows, D. N., et al. 2005, *Science*, 309, 1833.
- Butler, N. R., Kocevski, D., Bloom, J. S., & Curtis, J. L. 2007, *ApJ*, 671, 656.
- Bykov, A. M., Mészáros, P. 1996, *ApJ*, 461, L37
- Chevalier, R. A., & Li, Z.-Y. 2000, *ApJ*, 536, 195.
- Chincarini, G., et al. 2007, *ApJ*, 671, 1903.
- Cho, J., Lazarian, A., & Vishniac, E. T. 2002, *ApJ*, 564, 291.
- Coburn, W., & Boggs, S. E. 2003, *Nature*, 423, 415.
- Dai, Z. G., & Lu, T. 1998, *MNRAS*, 298, 87.
- Daigne, F., & Mochkovitch, R. 1998, *MNRAS*, 296, 275.
- Daughton, W., Scudder, J., & Karimabadi, H. 2006, *Physics of Plasmas*, 13(7), 072101.
- de Gouveia dal Pino, E. M., & Lazarian, A. 2005, *A&A*, 441, 845.
- Derishev, E. V., Kocharovsky, V. V., & Kocharovsky, V. V. 2001, *A&A*, 372, 1071.
- Dermer, C. D., & Mitman, K. E. 1999, *ApJ*, 513, L5.
- Drake, J. F., Swisdak, M., Che, H., Shay, M. A. *Nature*, 7111, 553
- Drenkhahn, G. 2002, *A&A*, 387, 714.
- Drenkhahn, G., & Spruit, H. C. 2002, *A&A*, 391, 1141.
- Falcone, A. D., et al. 2006, *ApJ*, 641, 1010.
- Falcone, A. D., et al. 2007, *ApJ*, 671, 1921.
- Fan, Y., Zhang, B., & Wei, D. 2009, *Phys. Rev. D*, 79(2), 021301.
- Fan, Y.-Z., Dai, Z.-G., Huang, Y.-F., & Lu, T. 2002, *Chinese Journal of Astronomy and Astrophysics*, 2, 449.
- Fan, Y. Z., & Wei, D. M. 2005, *MNRAS*, 364, L42.
- Fan, Y. Z., Wei, D. M., & Wang, C. F. 2004a, *A&A*, 424, 477.
- Fan, Y. Z., Wei, D. M., & Zhang, B. 2004b, *MNRAS*, 354, 1031.
- Fan, Y.-Z. 2010, *MNRAS*, 403, 483.
- Ford, L. A., et al. 1995, *ApJ*, 439, 307.
- Gao, W., Mao, J., Xu, D., & Fan, Y. 2009, *ApJ*, 706, L33.
- Ghirlanda, G., Nava, L., Ghisellini, G., Celotti, A., & Firmani, C. 2009, *A&A*, 496, 585.
- Ghisellini, G., & Celotti, A. 1999, *ApJ*, 511, L93.
- Ghisellini, G., Celotti, A., Ghirlanda, G., Firmani, C., & Nava, L. 2007, *MNRAS*, 382, L72.
- Ghisellini, G., Celotti, A., & Lazzati, D. 2000, *MNRAS*, 313, L1.
- Ghisellini, G., Ghirlanda, G., Nava, L., & Celotti, A. 2010, *MNRAS*, 403, 926.
- Giannios, D. 2008, *A&A*, 480, 305.
- Giannios, D., Mimica, P, Aloy, M. A. 2008, *A&A*, 478, 747
- Giannios, D., & Spitkovsky, A. 2009, *MNRAS*, 400, 330.
- Giannios, D., & Spruit, H. C. 2007, *A&A*, 469, 1.
- Giannios, D., Uzdensky, D. A., & Begelman, M. C. 2009, *MNRAS*, 395, L29.
- Goldreich, P., & Sridhar, S. 1995, *ApJ*, 438, 763.
- Golenetskii, S. V., Mazets, E. P., Aptekar, R. L., & Ilinskii, V. N. 1983, *Nature*, 306, 451.
- Gomboc, A., et al. 2008, *ApJ*, 687, 443.
- Goodman, J. 1986, *ApJ*, 308, L47.
- Granot, J. 2003, *ApJ*, 596, L17.
- Granot, J., Komissarov, S., Spitkovsky, A. 2010, *MNRAS*, in press (arXiv:1004.0959)
- Guetta, D., Spada, M., & Waxman, E. 2001, *ApJ*, 557, 399.
- Gupta, N., & Zhang, B. 2007, *A&A*, 477, 386.
- Gupta, N., & Zhang, B. 2008, *MNRAS*, 384, L11.
- Hill, J. E., et al. 2008. In Y.-F. Huang, Z.-G. Dai, & B. Zhang (Ed.), *American Institute of Physics Conference Series*, Volume 1065 of *American Institute of Physics Conference Series*, pp. 331–337.
- Jackson, J. D. 1975. *Classical electrodynamics*.
- Jin, Z. P., & Fan, Y. Z. 2007, *MNRAS*, 378, 1043.
- Kalemci, E., Boggs, S. E., Kouveliotou, C., Finger, M., & Baring, M. G. 2007, *ApJS*, 169, 75.
- Kobayashi, S., Piran, T., & Sari, R. 1997, *ApJ*, 490, 92.
- Kobayashi, S., Ryde, F., & MacFadyen, A. 2002, *ApJ*, 577, 302.
- Kobayashi, S., & Sari, R. 2001, *ApJ*, 551, 934.
- Kobayashi, S., Zhang, B., Mészáros, P., & Burrows, D. 2007, *ApJ*, 655, 391.
- Komissarov, S. S., Vlahakis, N., Königl, A., & Barkov, M. V. 2009, *MNRAS*, 394, 1182.
- Kowal, G., Lazarian, A., Vishniac, E. T., Otmianowska-Mazur, K. 2009, *ApJ*, 700, 63
- Krimm, H. A., et al. 2007, *ApJ*, 665, 554.
- Kumar, P. 1999, *ApJ*, 523, L113.
- Kumar, P., & Barniol Duran, R. 2009, *MNRAS*, 400, L75.
- Kumar, P., & Barniol Duran, R. 2010, *MNRAS*, 409, 226.
- Kumar, P., & McMahon, E. 2008, *MNRAS*, 384, 33.
- Kumar, P., et al. 2007, *MNRAS*, 376, L57.
- Kumar, P., & Narayan, R. 2009, *MNRAS*, 395, 472.
- Kumar, P., & Panaitescu, A. 2003, *MNRAS*, 346, 905.
- Kumar, P., & Panaitescu, A. 2008, *MNRAS*, 391, L19.
- Lamanna, G., et al. 2008. In *Polarimetry days in Rome: Crab status, theory and prospects*, published online at <http://pos.sissa.it/cgi-bin/reader/conf.cgi?confid=78>, p.22.
- Lazarian, A., Opher, M. 2009, *ApJ*, 703, 8
- Lazarian, A., Petrosian, V., Yan, H., & Cho, J. 2003, Review at the NBSI workshop "Beaming and Jets in Gamma Ray Bursts", Copenhagen, astro-ph/0301181
- Lazarian, A., & Vishniac, E. T. 1999, *ApJ*, 517, 700.
- Lazzati, D., Morsony, B. J., & Begelman, M. C. 2009, *ApJ*, 700, L47.
- Lazzati, D., & Perna, R. 2007, *MNRAS*, 375, L46.
- Lazzati, D. & Begelman, M. 2010, *ApJ*, 725, 1137.
- Levinson, A. 2010, *ApJ*, 720, 1490.
- Li, Z., 2010a, *ApJ*, 709, 525.
- Li, Z., 2010b, *ApJ*, submitted (arXiv:1004.0791).
- Liang, E. W., Dai, Z. G., & Wu, X. F. 2004, *ApJ*, 606, L29.
- Liang, E. W., et al. 2006, *ApJ*, 646, 351.
- Liang, E., Zhang, B., Virgili, F. Dai, Z. G. 2007, *ApJ*, 662, 1111
- Liang, E.-W., Yi, S.-X., Zhang, J., Lü, H.-J., Zhang, B.-B., & Zhang, B. 2010, *ApJ*, in press (arXiv:0912.4800)
- Loureiro, N. F., Schekochihin, A. A., Cowley, S. C. 2007, *Phys. Plasma*, 14, 100703
- Loureiro, N. F., Uzdensky, D. A., Schekochihin, A. A., Cowley, S. C., Yousef, T. A. 2009, *MNRAS*, 399, L146
- Lu, R.-J., Hou, S.-J., Liang, E.-W. 2010, *ApJ*, 718, 63
- Lyubarsky, Y. E. 2005, *MNRAS*, 358, 113.
- Lyubarsky, Y. E. 2010, *MNRAS*, 402, 353.
- Lyutikov, M. 2006a, *MNRAS*, 369, L5.
- Lyutikov, M. 2006b, *New Journal of Physics*, 8, 119.
- Lyutikov, M., & Blandford, R. 2003, preprint (arXiv:astro-ph/0312347)
- Lyutikov, M., Pariev, V. I., & Blandford, R. D. 2003, *ApJ*, 597, 998.
- Lyutikov, M., & Uzdensky, D. 2003, *ApJ*, 589, 893.
- MacFadyen, A. I., & Woosley, S. E. 1999, *ApJ*, 524, 262.
- Maxham, A., & Zhang, B. 2009, *ApJ*, 707, 1623.
- McGlynn, S., et al. 2007, *A&A*, 466, 895.
- Medvedev, M. V. 2000, *ApJ*, 540, 704.
- Medvedev, M. V. 2006, *ApJ*, 651, L9.
- Medvedev, M. V., & Loeb, A. 1999, *ApJ*, 526, 697.
- Mészáros, P., Ramirez-Ruiz, E., Rees, M. J., & Zhang, B. 2002, *ApJ*, 578, 812.
- Mészáros, P., & Rees, M. J. 1993, *ApJ*, 405, 278.

- Mészáros, P., & Rees, M. J. 1997a, *ApJ*, 476, 232.
Mészáros, P., & Rees, M. J. 1997b, *ApJ*, 482, L29.
Mészáros, P., & Rees, M. J. 2000, *ApJ*, 530, 292.
Mészáros, P., Rees, M. J., & Papathanassiou, H. 1994, *ApJ*, 432, 181.
Mészáros, P., Rees, M. J., & Wijers, R. A. M. J. 1998, *ApJ*, 499, 301.
Michel, F. C. 1969, *ApJ*, 158, 727.
Mimica, P., Giannios, D., & Aloy, M. A. 2009, *A&A*, 494, 879.
Mizuno, T., et al. 2005, *Nuclear Instruments and Methods in Physics Research A*, 540, 158.
Mizuno, Y., Zhang, B., Giacomazzo, B., Nishikawa, K.-I., Hardee, P. E., Nagataki, S., & Hartmann, D. H. 2009a, *ApJ*, 690, L47
Mizuno, Y., Lyubarsky, Y., Nishikawa, K.-I., Hardee, P. E. 2009b, 700, 684
Mundell, C. G., et al. 2007, *Science*, 315, 1822.
Murase, K., Ioka, K., Nagataki, S., Nakamura, T. 2006, *ApJ*, 651, L5
Murase, K., Ioka, K., Nagataki, S., Nakamura, T. 2008, *Phys. Rev. D*, 78, 023005
Muslimov, A. G., & Tsygan, A. I. 1992, *MNRAS*, 255, 61.
Nagataki, S. 2009, *ApJ*, 704, 937.
Nakar, E., & Piran, T. 2004, *MNRAS*, 353, 647.
Nakar, E., & Piran, T. 2005, *MNRAS*, 360, L73.
Narayan, R., & Kumar, P. 2009, *MNRAS*, 394, L117.
Nishikawa, K.-I., Hardee, P., Richardson, G., Preece, R., Sol, H., & Fishman, G. J. 2005, *ApJ*, 622, 927.
Nishikawa, K.-I., et al. 2009, *ApJ*, 698, L10.
Nobili, L., Turolla, R., Zane, S. 2008, *MNRAS*, 386, 1527
Norris, J. P., Share, G. H., Messina, D. C., Dennis, B. R., Desai, U. D., Cline, T. L., Matz, S. M., & Chupp, E. L. 1986, *ApJ*, 301, 213
O'Brien, P. T., et al. 2006, *ApJ*, 647, 1213.
Paczynski, B. 1986, *ApJ*, 308, L43.
Paczynski, B., & Xu, G. 1994, *ApJ*, 427, 708.
Panaitescu, A., & Mészáros, P. 2000, *ApJ*, 544, L17.
Panaitescu, A., Spada, M., & Mészáros, P. 1999, *ApJ*, 522, L105.
Parker, E. N. 1957, *J. Geophys. Res.*, 62, 509.
Pe'er, A. 2008, *ApJ*, 682, 463.
Pe'er, A., Mészáros, P., & Rees, M. J. 2006, *ApJ*, 642, 995.
Pe'er, A., & Zhang, B. 2006, *ApJ*, 653, 454.
Pe'er, A., Zhang, B.-B., Ryde, F., McGlynn, S., Zhang, B., Preece, R. D. & Kouveliotou, C., 2010, *ApJ*, submitted (arXiv:1007.2228)
Petschek, H. E. 1964, *NASA Special Publication*, 50, 425.
Piran, T., & Nakar, E. 2010, (arXiv:1003.5919).
Piran, T., Sari, R., & Zou, Y.-C. 2009, *MNRAS*, 393, 1107.
Preece, R. D., Briggs, M. S., Malozzi, R. S., Pendleton, G. N., Paciesas, W. S., & Band, D. L. 2000, *ApJS*, 126, 19.
Proga, D., MacFadyen, A. I., Armitage, P. J., Begelman, M. C. 2003, *ApJ*, 599, L5
Racusin, J. L., et al. 2008, *Nature*, 455, 183.
Razzaque, S., Dermer, C. D., Finke, J. D. 2010, *The Open Astronomy Journal*, 3, 150 (arXiv:0905.1115)
Rees, M. J., & Mészáros, P. 1992, *MNRAS*, 258, 41P.
Rees, M. J., & Mészáros, P. 1994, *ApJ*, 430, L93.
Rees, M. J., & Mészáros, P. 2005, *ApJ*, 628, 847.
Resmi, L., Zhang, B. 2010, *MNRAS*, submitted
Romano, P., et al. 2006, *A&A*, 450, 59.
Rossi, E., Lazzati, D., & Rees, M. J. 2002, *MNRAS*, 332, 945.
Rutledge, R. E., & Fox, D. B. 2004, *MNRAS*, 350, 1288.
Rybicki, G. B., & Lightman, A. P. 1979. *Radiative processes in astrophysics*. New York, Wiley-Interscience, 1979. 393 p.
Ryde, F. 2005, *ApJ*, 625, L95.
Ryde, F., & Pe'er, A. 2009, *ApJ*, 702, 1211.
Ryde, F. et al. 2010, *ApJ*, 709, 172.
Sari, R., & Piran, T. 1995, *ApJ*, 455, L143.
Sari, R., & Piran, T. 1997, *ApJ*, 485, 270.
Sari, R., Piran, T., & Narayan, R. 1998, *ApJ*, 497, L17.
Shemi, A., & Piran, T. 1990, *ApJ*, 365, L55.
Shen, R., & Song, L. 2003, *PASJ*, 55, 345.
Shen, R., & Zhang, B. 2009, *MNRAS*, 398, 1936.
Sironi, L., & Spitkovsky, A. 2009, *ApJ*, 707, L92.
Spitkovsky, A. 2008, *ApJ*, 682, L5.
Spitzer, L. 1962, *Physics of Fully Ionized Gases*, New York: Interscience (2nd edition).
Spruit, H. C., Daigne, F., & Drenkhahn, G. 2001, *A&A*, 369, 694.
Steele, I. A., Mundell, C. G., Smith, R. J., Kobayashi, S., & Guidorzi, C. 2009, *Nature*, 462, 767.
Stern, B. E., & Poutanen, J. 2004, *MNRAS*, 352, L35.
Sweet, P. A. 1958. In B. Lehnert (Ed.), *Electromagnetic Phenomena in Cosmical Physics*, Volume 6 of *IAU Symposium*, pp. 123–+.
Tagliaferri, G., et al. 2005, *Nature*, 436, 985.
Tavani, M. 1996, *ApJ*, 466, 768.
Tchekhovskoy, A., McKinney, J. C., & Narayan, R. 2008, *MNRAS*, 388, 551.
Thompson, C. 1994, *MNRAS*, 270, 480.
Thompson, C. 2006, *ApJ*, 651, 333.
Thompson, C., Mészáros, P., & Rees, M. J. 2007, *ApJ*, 666, 1012.
Toma, K., Wu, X.-F., & Mészáros, P. 2009a, *ApJ*, 707, 1404.
Toma, K., et al. 2009b, *ApJ*, 698, 1042.
Toma, K., Wu, X.-F., & Mészáros, P. 2010, *MNRAS*, submitted (arXiv:1002.2634)
Usov, V. V. 1992, *Nature*, 357, 472.
Uzdensky, D. A., & Kulsrud, R. M. 2000, *Physics of Plasmas*, 7, 4018.
Vetere, L., Massaro, E., Costa, E., Soffitta, P., & Ventura, G. 2006, *A&A*, 447, 499
Virgili, F., Liang, E.-W., Zhang, B. 2009, *MNRAS*, 392, 91
Vlahakis, N., & Königl, A. 2003, *ApJ*, 596, 1080.
Wang, X., Li, Z., Dai, Z., & Mészáros, P. 2009, *ApJ*, 698, L98.
Waxman, E. 1995, *Physical Review Letters*, 75, 386.
Waxman, E. 2003, *Nature*, 423, 388.
Waxman, E., & Bahcall, J. 1997, *Physical Review Letters*, 78, 2292.
Wei, D. M., & Gao, W. H. 2003, *MNRAS*, 345, 743.
Weibel, E. S. 1959, *Physical Review Letters*, 2, 83.
Wheeler, J. C., Yi, I., Höflich, P., & Wang, L. 2000, *ApJ*, 537, 810.
Wigger, C., Hajdas, W., Arzner, K., Güdel, M., & Zehnder, A. 2004, *ApJ*, 613, 1088.
Willis, D. R., et al. 2005, *A&A*, 439, 245.
Woosley, S. E. 1993, *ApJ*, 405, 273.
Yonetoku, D., Murakami, T., Nakamura, T., Yamazaki, R., Inoue, A. K., & Ioka, K. 2004, *ApJ*, 609, 935.
Zenitani, S., Hesse, M., Klimas, A., *ApJ*, 696, 1385
Zenitani, S., Hesse, M., Klimas, A., *ApJ*, 716, 214
Zhang, B., Fan, Y. Z., Dyks, J., Kobayashi, S., Mészáros, P., Burrows, D. N., Nousek, J. A., & Gehrels, N. 2006, *ApJ*, 642, 354
Zhang, B., & Kobayashi, S. 2005, *ApJ*, 628, 315.
Zhang, B., Kobayashi, S., & Mészáros, P. 2003, *ApJ*, 595, 950.
Zhang, B., et al. 2007, *ApJ*, 655, 989.
Zhang, B., & Mészáros, P. 2002a, *ApJ*, 581, 1236.
Zhang, B., & Mészáros, P. 2002b, *ApJ*, 571, 876.
Zhang, B., & Pe'er, A. 2009, *ApJ*, 700, L65.
Zhang, B.-B., Liang, E.-W., & Zhang, B. 2007, *ApJ*, 666, 1002.
Zhang, B.-B., Zhang, B., Liang, E.-W., & Wang, X.-Y. 2009a, *ApJ*, 690, L10.
Zhang, B.-B., Zhang, B., Liang, E.-W. et al. 2010, *ApJ*, submitted (arXiv:1009.3338)
Zhang, W., MacFadyen, A., & Wang, P. 2009b, *ApJ*, 692, L40.
Zou, Y., Piran, T., & Sari, R. 2009, *ApJ*, 692, L92.

Notes added in proof: After acceptance of our paper, we were notified by Jon McKinney about an alternative mechanism to trigger fast reconnection at large radii of GRBs (J. C. McKinney & D. A. Uzdensky, *MNRAS*, submitted, arXiv:1011.1904).

Distance Scales in the ICMART Model

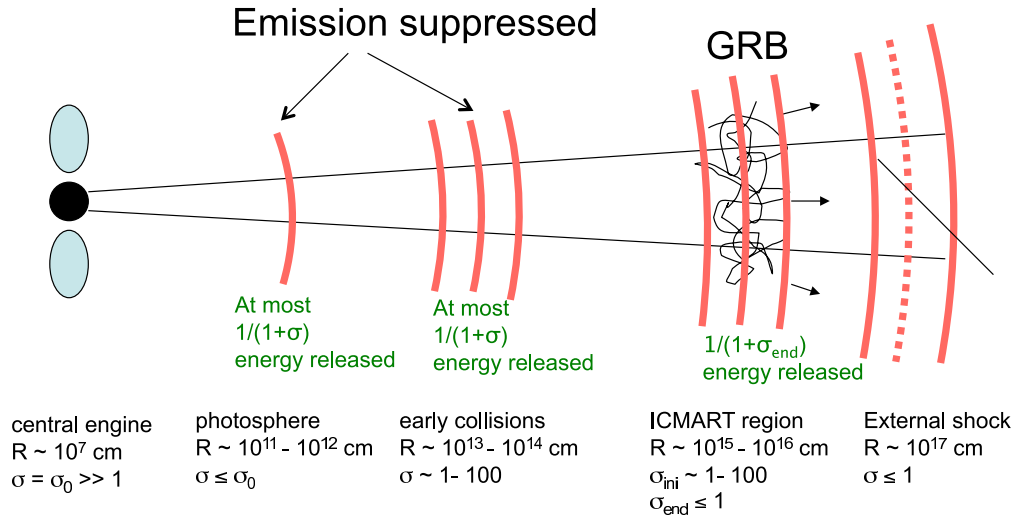


FIG. 1.— A cartoon picture of the ICMART model. The typical distances and σ values of various events are marked.

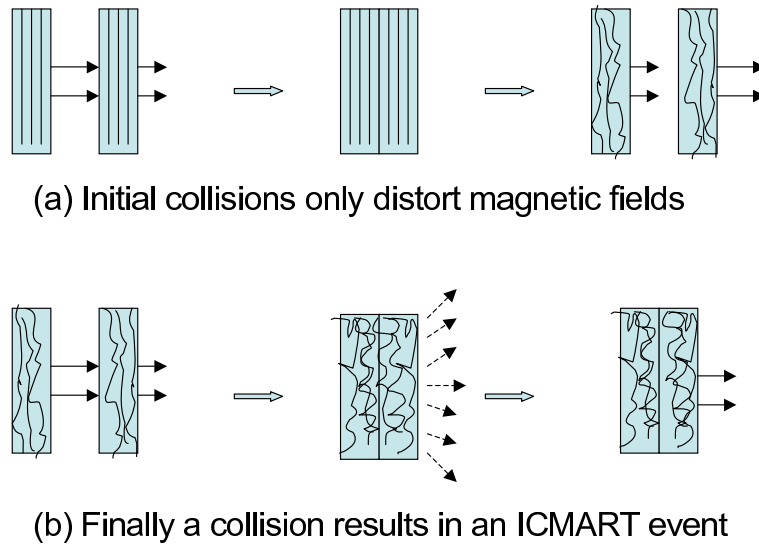


FIG. 2.— Examples of internal collisions that mainly distort magnetic fields and result in catastrophic discharge of magnetic energy in an ICMART event.

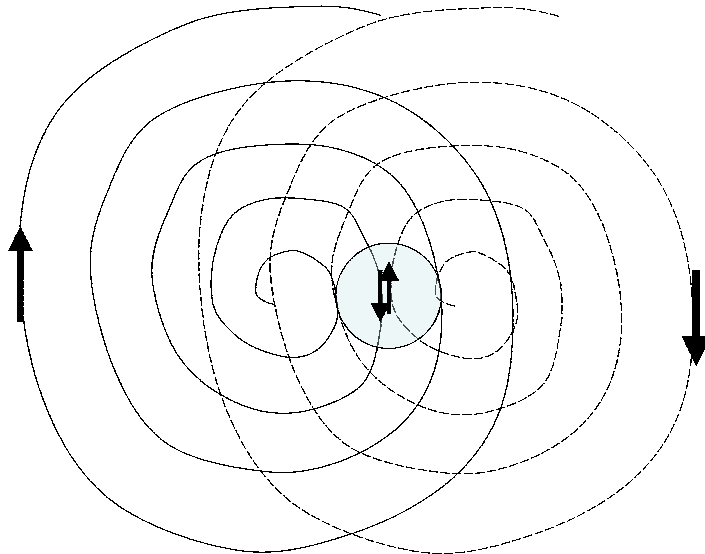


FIG. 3.— An example of triggering an ICMART event. Magnetic field lines with opposite orientations can approach each other and may result in fast reconnection to trigger ICMART if the two shells with mis-aligned helical magnetic field configuration collide.

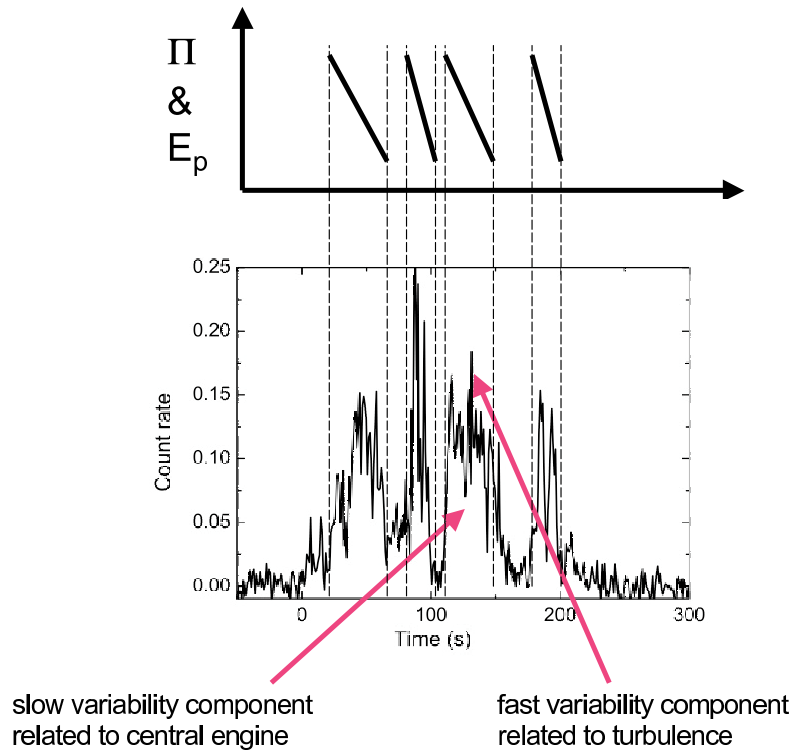


FIG. 4.— An example of GRB light curve that shows two variability time scales. The light curve of GRB 050117 is extracted from the UNLV GRB group website <http://grb.physics.unlv.edu/~xrt/xrtweb/050117/050117.html>. The predictions of decreasing gamma-ray polarization degree Π and the spectral peak energy E_p within individual pulses are indicatively presented. Detailed decaying functions would be different depending on the details of evolution of magnetic field configuration, σ value, as well as balance between heating and cooling of electrons. The general decreasing trend is robust.